

เซอร์เฟซเอ็นฮานซ์รามานสแกตเทอริงที่ใช้อนุภาคระดับนาโนเมตรของโลหะ  
สำหรับการตรวจวัดคาร์โบฟูแรน



นางสาวธัญญาดา สุขมณี

บทคัดย่อและแฟ้มข้อมูลฉบับเต็มของวิทยานิพนธ์ตั้งแต่ปีการศึกษา 2554 ที่ให้บริการในคลังปัญญาจุฬาฯ (CUIR)  
เป็นแฟ้มข้อมูลของนิสิตเจ้าของวิทยานิพนธ์ ที่ส่งผ่านทางบัณฑิตวิทยาลัย

The abstract and full text of theses from the academic year 2011 in Chulalongkorn University Intellectual Repository (CUIR)  
are the thesis authors' files submitted through the University Graduate School.

วิทยานิพนธ์นี้เป็นส่วนหนึ่งของการศึกษาตามหลักสูตรปริญญาวิทยาศาสตรมหาบัณฑิต  
สาขาวิชาเคมี ภาควิชาเคมี  
คณะวิทยาศาสตร์ จุฬาลงกรณ์มหาวิทยาลัย  
ปีการศึกษา 2558  
ลิขสิทธิ์ของจุฬาลงกรณ์มหาวิทยาลัย

SURFACE ENHANCED RAMAN SCATTERING USING METAL NANOPARTICLES  
FOR CARBOFURAN DETECTION

Miss Thanyada Sukmanee



A Thesis Submitted in Partial Fulfillment of the Requirements  
for the Degree of Master of Science Program in Chemistry

Department of Chemistry

Faculty of Science

Chulalongkorn University

Academic Year 2015

Copyright of Chulalongkorn University

Thesis Title	SURFACE ENHANCED RAMAN SCATTERING USING METAL NANOPARTICLES FOR CARBOFURAN DETECTION
By	Miss Thanyada Sukmanee
Field of Study	Chemistry
Thesis Advisor	Assistant Professor Kanet Wongravee, Ph.D.
Thesis Co-Advisor	Prompong Pienpinijtham, Ph.D.

---

Accepted by the Faculty of Science, Chulalongkorn University in Partial Fulfillment of the Requirements for the Master's Degree

.....Dean of the Faculty of Science  
(Associate Professor Polkit Sangvanich, Ph.D.)

#### THESIS COMMITTEE

.....Chairman  
(Associate Professor Vudhichai Parasuk, Ph.D.)

.....Thesis Advisor  
(Assistant Professor Kanet Wongravee, Ph.D.)

.....Thesis Co-Advisor  
(Prompong Pienpinijtham, Ph.D.)

.....Examiner  
(Assistant Professor Sumrit Wacharasindhu, Ph.D.)

.....External Examiner  
(Nattawadee Wisitruangsakul, Ph.D.)

ัญญาดา สุขมณี : เซอร์เฟซเอ็นฮานซ์รามานสแกตเทอริงที่ใช้อนุภาคระดับนาโนเมตรของโลหะสำหรับการตรวจวัดคาร์โบฟูแรน (SURFACE ENHANCED RAMAN SCATTERING USING METAL NANOPARTICLES FOR CARBOFURAN DETECTION) อ.ที่ปรึกษาวิทยานิพนธ์หลัก: ผศ. ดร.คณิศ วังษะระวี, อ.ที่ปรึกษาวิทยานิพนธ์ร่วม: ดร.พร้อมพงศ์ เพียรพินิจธรรม, หน้า.

อนุภาคระดับนาโนเมตรของโลหะเงินถูกใช้อย่างแพร่หลายเพื่อเป็นซับสเตรต (substrate) สำหรับใช้เพิ่มสัญญาณรามานของโมเลกุลที่อยู่ใกล้พื้นผิวของอนุภาค เป็นการเพิ่มศักยภาพในการตรวจวัดด้วยเทคนิคเซอร์เฟซเอ็นฮานซ์รามานสแกตเทอริง (surface enhanced Raman scattering, SERS) งานวิจัยนี้มุ่งเน้นที่จะพัฒนาวิธีการตรวจวัดคาร์โบฟูแรนซึ่งเป็นยาฆ่าแมลงชนิดคาร์บาเมทเอสเทอร์ชนิดหนึ่งที่มีความเป็นพิษสูง โดยอาศัยปฏิกิริยาคู่ควบ (coupling reaction) ของไดอะโซเนียมไอออน (diazonium ion) ร่วมกับเทคนิคเซอร์เฟซเอ็นฮานซ์รามานสแกตเทอริง เพื่อการตรวจวัดที่มีสภาพไวและมีความจำเพาะเจาะจงสูง ไดอะโซเนียมไอออนจะทำปฏิกิริยาอย่างจำเพาะเจาะจงกับคาร์โบฟูแรนฟีนอล (carbofuran phenol) ที่ได้จากปฏิกิริยาไฮโดรไลซิสของคาร์โบฟูแรนโดยมีเบสเป็นตัวเร่งปฏิกิริยา (alkali-catalyzed hydrolysis) จะได้สารประกอบเอโซ (azo compound) เป็นผลิตภัณฑ์ สำหรับการวิเคราะห์ด้วยเทคนิคเซอร์เฟซเอ็นฮานซ์รามานสแกตเทอริง โมเลกุลของสารประกอบเอโซที่ได้นั้นจะติดอยู่บนพื้นผิวของอนุภาคระดับนาโนเมตรของโลหะเงินผ่านพันธะโคเวเลนต์ที่แข็งแรงของ Ag-S ทำให้สามารถตรวจพบสัญญาณรามานที่มีความเข้มสูงได้ ในการวิเคราะห์ปริมาณคาร์โบฟูแรน ผู้วิจัยทำการสร้างกราฟเส้นตรงแสดงความสัมพันธ์ระหว่างอัตราส่วนความเข้มของสัญญาณรามานที่ 1201 และ 1021  $\text{cm}^{-1}$  ต่อความเข้มข้นของคาร์โบฟูแรน ในช่วง 0.1–5 ppm จะได้ค่า  $R^2 = 0.9891$  และค่าความเข้มข้นต่ำสุดที่ 0.729 ppm นอกจากนี้วิธีการวิเคราะห์คาร์โบฟูแรนนี้จะไม่ถูกรบกวนจากกรดโมเลกุลเล็ก (กรดธรรมชาติ) น้ำตาลโมเลกุลเดี่ยวและน้ำตาลทราย วิธีวิเคราะห์ที่พัฒนาขึ้นนี้ยังนำไปใช้ในการตรวจวัดปริมาณคาร์โบฟูแรนที่ตกค้างในผลิตภัณฑ์ทางการเกษตร เช่น ข้าว ถั่วเหลือง พริกไทยขาว พริกไทยดำ ถั่วเขียว งา ถั่วลิสง และพริกแห้ง เป็นต้น

ภาควิชา	เคมี	ลายมือชื่อนิสิต .....
สาขาวิชา	เคมี	ลายมือชื่อ อ.ที่ปรึกษาหลัก .....
ปีการศึกษา	2558	ลายมือชื่อ อ.ที่ปรึกษาร่วม .....

# # 5671984123 : MAJOR CHEMISTRY

KEYWORDS: SERS / SILVER NANOPARTICLES / CARBOFURAN / COUPLING REACTION

THANYADA SUKMANEE: SURFACE ENHANCED RAMAN SCATTERING USING METAL NANOPARTICLES FOR CARBOFURAN DETECTION. ADVISOR: ASST. PROF. KANET WONGRAVEE, Ph.D., CO-ADVISOR: PROMPONG PIENPINIJTHAM, Ph.D., pp.

Silver nanoparticles (AgNPs) have been widely used as substrates to enhance Raman signals of molecules oriented nearby the AgNPs surface. This improves the detection limit via surface-enhanced scattering (SERS) technique. In this research, the coupling reaction of diazonium ion combined with SERS provides a selective and sensitive detection method for trace analysis of carbofuran, which is one of the most toxic carbamate insecticides. Diazonium ion specifically reacts with carbofuran phenol created from the alkaline hydrolysis of carbofuran to generate azo dye complex. In SERS measurement, the generated azo compound is easily deposited on the surface of AgNPs by strong Ag-S bond; therefore, the strong Raman intensity of the azo dye can be observed. To quantify carbofuran, the ratio of Raman intensity at  $1201\text{ cm}^{-1}$  over  $1021\text{ cm}^{-1}$  were linearly plotted against the concentrations of carbofuran with  $R^2 = 0.9891$  in the range of 0.1–5 ppm. The limit of detection (LOD) is 0.729 ppm. Moreover, our proposed carbofuran detection method was insignificantly influenced by interferences e.g., small acid molecules and monosaccharide sugars. For practical analysis, the developed method of carbofuran detection was also studied in real agricultural products (e.g., rice, beans, peppers, sesame).

Department: Chemistry

Field of Study: Chemistry

Academic Year: 2015

Student's Signature .....

Advisor's Signature .....

Co-Advisor's Signature .....

## ACKNOWLEDGEMENTS

First and foremost, this thesis has been successfully completed by the great guidance, generous training and considerate understanding of my thesis advisors and the kind supporting of our laboratory member. I would like to appreciatively express my gratitude to my thesis advisor, Assistant Professor Dr. Kanet Wongravee, my thesis co-advisor, Dr. Prompong Pienpinijtham, Professor Dr. Sanong Ekgasit, Associate Professor Chuchaat Thammacharoen for kind suggestion and detailed direction in the scientific knowledge and practical laboratory techniques.

I would like to sincerely thank Associate Professor Dr. Vudhichai Parasuk, Assistant Professor Dr. Sumrit Wacharasindhu and Dr. Nattawadee Wisitruangsakul for being my thesis committee with thoughtful and useful suggestions.

I would also like to gratefully thank to my colleagues and organization: Sensor Research Unit (SRU), Department of Chemistry, Faculty of science, Chulalongkorn University for hospitable supporting and powerful encouragement throughout this research.

The financial support from the Development and Promotion of Science and Technology Talents Project (DPST) to Thanyada Sukmanee is gratefully acknowledged. This research also has financial supports from the Thailand Research Fund (TRG5780158) and National Research University Project, Office of Higher Education Commission (WCU-018-FW-57).

Above all, I would like to thank my family: my parents and to my brother and sister for supporting me spiritually throughout writing this thesis and my life in general.

## CONTENTS

	Page
THAI ABSTRACT .....	iv
ENGLISH ABSTRACT .....	v
ACKNOWLEDGEMENTS .....	vi
CONTENTS .....	vii
LIST OF TABLES .....	ix
LIST OF FIGURES .....	x
LIST OF ABBREVIATION AND SYMBOLS .....	xiii
CHAPTER I INTRODUCTION.....	1
1.1 Carbofuran.....	1
1.2 Conventional method for pesticide detection .....	2
1.3 Surface-enhanced Raman spectroscopy (SERS) for pesticide detection.....	3
1.4 The objectives .....	5
1.5 Scopes of this research.....	6
CHAPTER 2 THEORETICAL BACKGROUND.....	7
2.1 Raman spectroscopy.....	7
2.2 Localized surface plasmon resonance (LSPR) .....	8
2.3 Surface-enhanced Raman spectroscopy (SERS) .....	10
2.4 Hydrolysis of carbofuran .....	11
2.5 Azo coupling reaction .....	13
CHAPTER 3 EXPERIMENTS .....	16
3.1 Chemicals and instruments .....	16
3.2 The synthesis of silver nanoparticles (AgNPs).....	16

	Page
3.3 The alkaline hydrolysis reaction of carbofuran .....	17
3.4 The preparation of azo compound using coupling reaction .....	17
3.5 SERS measurement .....	18
3.6 Effect of interfering substances on the detection method .....	19
3.7 Method validation of carbofuran detection in real samples.....	20
CHAPTER 4 RESULTS AND DISCUSSION.....	21
4.1 The synthesis of colloidal citrate-reduced silver nanoparticles .....	21
4.2 The interaction between carbofuran and AgNPs .....	22
4.3 The formation of azo compound.....	23
4.4 Carbofuran detection using surface enhanced Raman scattering .....	26
4.5 Effect of incubation time in alkaline hydrolysis reaction .....	30
4.6. Effect of 4-ATP concentration in diazotization reaction.....	32
4.7 Effect of incubation time in coupling reaction .....	35
4.8 Diazo-coupling-based SERS for carbofuran detection.....	37
4.9 Effect of interfering substances on the detection method .....	40
4.10 Carbofuran analysis in real samples using our developed method.....	42
CHAPTER 5 CONCLUSIONS.....	46
.....	48
REFERENCES .....	48
APPENDIX.....	55
VITA.....	61



## LIST OF TABLES

Table 1.1 Conventional methods for pesticide detection.....	3
Table 1.2 SERS technique for pesticide detection .....	5
Table 2.1 Half-life of carbofuran in degradation process.....	11
Table 4.1 SERS Peak Assignments for 4-mercaptophenol and azo compound.....	30
Table 4.2 Maximum residue limits (MRLs) of each agricultural product.....	44



## LIST OF FIGURES

Figure 2.1 Scheme of Rayleigh scattering and Raman scattering including (a) Stoke scattering and (b) Anti-Stoke scattering. ....	8
Figure 2.2 Schemes of (a) a surface plasmon polariton for planar interface and (b) a localized surface plasmon for nanoparticles [19] .....	10
Figure 2.3 Scheme of degradation process of carbofuran ; (a) carbofuran, (b) carbofuran phenol, (c) 3-hydroxy carbofuran, (d) 3-hydroxy carbofuran-7-phenol, (e) 3-keto carbofuran and (f) 3-keto carbofuran-7-phenol.....	12
Figure 2.4 Mechanism of coupling reaction for the formation of aryl azo compound.....	14
Figure 2.5 Structure of aromatic azo compound at (a) <i>para</i> -, (b) <i>ortho</i> -position ; where X is -NH <sub>2</sub> or -OH group and R can be both alkyl and aryl group.....	14
Figure 2.6 Mechanism of diazotization for the formation of diazonium ion.....	15
Figure 3.1 The alkaline hydrolysis reaction of carbofuran for generating carbofuran phenol.....	17
Figure 3.2 (a) The diazotization for preparing diazonium ion and (b) The diazo coupling reaction for generating the azo compound. ....	18
Figure 3.3 The deposition of azo compound on the surface of AgNPs. ....	19
Figure 4.1 Plasmonic extinction spectrum of synthesized colloidal AgNPs. ....	21
Figure 4.2 SERS spectra of (a) ethanol and (b) 1000 ppm carbofuran in ethanol. ....	22
Figure 4.3 The diazo coupling reaction to produce an azo compound with -SH group from carbofuran phenol.....	23
Figure 4.4 UV-visible spectra of the azo compounds generated using various carbofuran concentrations (0–1000 ppm). The inset demonstrates the corresponding solution color of azo compounds at various carbofuran concentrations.....	24

Figure 4.5 The correlation of carbofuran concentration (0.5–50 ppm) and absorbance at 480 nm. ....	25
Figure 4.6 Extinction spectra of AgNPs and AgNPs with azo compound. ....	26
Figure 4.7 Scheme of azo compound on the surface of silver nanoparticles.....	26
Figure 4.8 SERS spectra of (a) 1000 ppm carbofuran phenol and compounds from an azo coupling reaction using (b) 0 and (c) 100 ppm carbofuran. ....	28
Figure 4.9 The formation mechanism of 4-mercaptophenol on the surface of AgNPs.....	29
Figure 4.10 Alkali-catalyzed hydrolysis mechanism of carbofuran to carbofuran phenol.....	31
Figure 4.11 The relationship between Raman intensity at $1201\text{ cm}^{-1}$ and hydrolysis time. ....	32
Figure 4.12 Mechanism of diazotization for the formation of diazonium ion.....	33
Figure 4.13 SERS spectra of the azo compound generated using 100 ppm carbofuran phenol with various concentrations of 4-ATP: (a) 0.5, (b) 1, (c) 2 and (d) 3 mM, respectively (The incubation time of diazotization is 1 minute). ....	35
Figure 4. 14 Mechanism of diazo coupling reaction between carbofuran phenol and diazonium ion generated from 4-ATP. ....	36
Figure 4.15 The correlation of Raman intensity at $1201\text{ cm}^{-1}$ with the incubation time. ....	37
Figure 4.16 SERS spectra of azo compound generated from (a) 0, (b) 0.1, (c) 0.5, (d) 1, (e) 5, (f) 10, (g) 50, (h) 100, (i) 500 and (j) 1000 ppm carbofuran.....	39
Figure 4.17 The intensity ratios of $1201\text{ cm}^{-1} / 1021\text{ cm}^{-1}$ (A1) and $1201\text{ cm}^{-1} / 1075\text{ cm}^{-1}$ (B1) versus the concentration of carbofuran and the relation between the intensity ratios of $1201\text{ cm}^{-1} / 1021\text{ cm}^{-1}$ (A2) and $1201\text{ cm}^{-1} / 1075\text{ cm}^{-1}$ (B2) versus the concentration of carbofuran in the range of 0.1-5 ppm. ....	40

Figure 4.18 The intensity ratios between peaks at 1201 and 1021 $\text{cm}^{-1}$ from SERS spectra of azo compound generated from 5 ppm carbofuran in the presence of 1mM interfering substance. ....	41
Figure 4.19 The relation between the intensity ratios and concentration of carbofuran in the range of 0.1–5 ppm from agricultural products, <i>i.e.</i> , (a) rice, (b) soya bean, (c) white pepper, (d) black pepper, (e) mung bean, (f) sesame, (g) peanut, and (h) chili pepper. ....	43
Figure 4.20 The recovery percentage of 0.1 and 5 ppm carbofuran, which is spiked on the samples. ....	45



## LIST OF ABBREVIATION AND SYMBOLS

HPLC-MS	: high-performance liquid chromatography with mass spectrometry
LC-MS	: liquid chromatography with mass spectrometry
GC-MS	: gas chromatography with mass spectrometry
GC-NCI-MS	: gas chromatography-negative chemical ionization-mass spectrometry
CV	: cyclic voltammetry
EIS	: electrochemical impedance spectroscopy
RI	: refractive index
IR	: infrared
SEIR	: surface-enhanced infrared
SEIRA	: surface-enhanced infrared adsorption spectroscopy
SPFS	: surface-enhanced fluorescence spectroscopy
SERS	: surface-enhanced Raman spectroscopy
SPs	: surface plasmons
LSPR	: localized surface plasmon resonance
NPs	: metallic nanoparticles
AuNPs	: gold nanoparticles
AgNPs	: silver nanoparticles
AgNO <sub>3</sub>	: silver nitrates
Na <sub>3</sub> C <sub>6</sub> H <sub>5</sub> O <sub>7</sub>	: tri-sodium citrate
KOH	: potassium hydroxide
NaNO <sub>2</sub>	: sodium nitrite
C <sub>12</sub> H <sub>15</sub> NO <sub>3</sub>	: carbofuran

4-ATP, C<sub>6</sub>H<sub>7</sub>NS : 4-aminothiophenol

HCl : hydrochloric acid

C<sub>2</sub>H<sub>6</sub>O : ethanol

g : gram

mg : milligram

kg : kilogram

μg : microgram

ng : nanogram

L : liter

mL : milliliter

ppm : part per million

nm : nanometer

M : molar

mM : millimolar

mW : milliwatt

cps : counts per second

λ : wavelength

$\bar{\nu}$  : wavenumber

cm<sup>-1</sup> : reciprocal centimeters

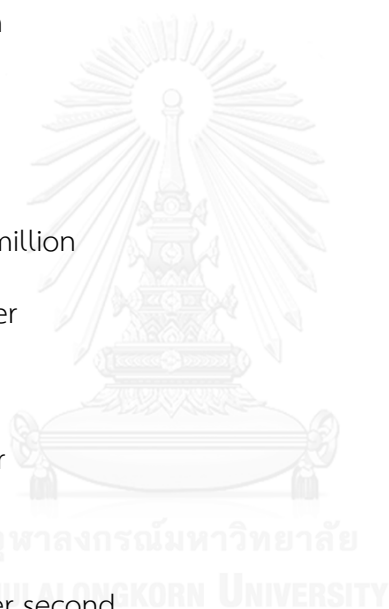
°C : degree Celsius

DI water : deionized water

UV : ultraviolet

LOD : limit of detection

MRLs : maximum residue limits



## CHAPTER I

### INTRODUCTION

As we know that Thailand is mostly an agricultural country, a large proportion of population have not only produced the agricultural and food products for their domestic consumption but also traded for the export industry. The agriculture in Thailand is in a highly competitive market. Therefore, Thailand imports a large amount of carbofuran per year to be used extensively in the agriculture, such as rice, banana, eggplant, corn, cabbage, soybean, watermelon, and other fruits and vegetables for higher quality and better yield [1]. As a matter of fact, the Thai government also concerns the high toxicity of carbofuran residues because it is a danger to human health, environment, and international trade. For the improvement of facilitating trade and protecting consumers, carbofuran is on the Thai government's dangerous chemicals watched list in order to carefully keep control of its contamination in environment and agricultural products. Maximum Residue Limit (MRL) of Thai agricultural standard is 0.1 mg/kg and that of European Commission is 0.02 mg/kg. Thus, the development of sensitive and selective detection method is urgently required to monitor and restrict the level of carbofuran residues for world food security.

#### 1.1 Carbofuran

Carbofuran is one of the most toxic carbamate insecticides, which is widely used worldwide in many varieties of field crops. Its trade names include Furadan, Carbodan, Carbosip, Chinofur, Curaterr, Furacarb, Kenafuran, Pillarfuron, Rampart, Nex, Bay 70143, D 1221, ENT 27164, and Yaltox. The plants can adsorb carbofuran rapidly through the roots from soil and transport to their organs but the metabolism of carbofuran in plants takes around 30 days to convert to non-toxic compound and carbofuran in soil is degraded by chemical hydrolysis and microbial process according to soil pH, clay content, temperature, moisture and microbial population for 26–378

days [2]. Nowadays, many countries, e.g., U.S., Canada, EU, Malaysia, Vietnam, Myanmar, Singapore *etc.*, have officially banned the use of carbofuran due to its high toxic activity as an anti-cholinesterase that inhibits the acetylcholinesterase in the nervous system [3, 4]. Moreover, the high toxicity of acetylcholinesterase inhibitor has resulted in muscular paralysis, convulsions, bronchial constriction, death by asphyxiation [5] and harmful effect in reproductive system for a long-term exposure [6].

## 1.2 Conventional method for pesticide detection

Nowadays, several highly sensitive conventional methods, e.g., high-performance liquid chromatography with mass spectrometry (HPLC-MS), liquid chromatography with mass spectrometry (LC-MS), and biosensor have been applied to detect pesticides. For instance, Zomer *et al.* designed and developed a rapid and sensitive test kit as bioluminescence method for the determination of carbamate and organophosphate pesticides with limit of detection below about 0.05 ppm [1]. Skla'dal *et al.* developed the biological method for carbamate pesticides detection by using cholinesterase as biosensor and the detection limit is at the level of 0.01 ppm [3]. Li *et al.* applied gas chromatography with mass spectrometry (GC-MS) to monitor the amount of organophosphate pesticides in surface water with detection limit between  $0.7\text{--}50 \times 10^{-3}$  ppm [7]. Sun *et al.* investigated the carbofuran analysis by using cyclic voltammetry (CV) and electrochemical impedance spectroscopy (EIS) with anti-carbofuran monoclonal antibody immobilized on glassy carbon electrode. The detection limit of this method is  $0.33 \times 10^{-3}$  ppm [4]. Nelson and co-workers determined the residues of the phenolic metabolites of carbofuran in plants using gas chromatographic procedure combined with mass spectrometry. Their method is sensitive in the range of 0.05–0.10 ppm with the average recoveries of the phenolic metabolites ranged from 72 to 104 % [8]. Zhu *et al.* analyzed organochlorine pesticide and pyrethroids in Chinese tea by screening and confirmatory detection using gas chromatography-negative chemical ionization-mass spectrometry (GC-NCI-MS) and gas chromatography tandem mass spectrometry (GC-MS/MS). The detection



limit of these techniques are in the range of 0.02–4.5 and 0.1–5.0  $\mu\text{g}/\text{kg}$  for GC-NCI-MS and GC-MS/MS, respectively [9]. However, all of these methods are in need of complicated processes, expensive instruments, long analysis time, and sample pretreatments. For this reason, a simple, rapid, sensitive, and selective detection technique for carbofuran is necessary and challenging in practical applications.

Table 1.1 Conventional methods for pesticide detection

Year	Researchers	Technique	Type of pesticide	Detection limit
1994	Zomer <i>et al.</i>	Bioluminescence	Organophosphate and carbamate	$\leq 0.05$ ppm
1997	Skla'dal <i>et al.</i>	Biosensor (Cholinesterase, current measurement)	Carbamate	0.01 ppm
2010	Li <i>et al.</i>	GC-MS	Organophosphate	$0.7\text{--}50 \times 10^{-3}$ ppm
2011	Sun <i>et al.</i>	Biosensor (Anti-carbofuran monoclonal antibody, CV - EIS)	Carbofuran	$0.33 \times 10^{-3}$ ppm
2013	Funari <i>et al.</i>	Biosensor (Quartz Crystal Microbalance, QCM)	Parathion	0.06 ppm
2014	Zhu <i>et al.</i>	GC - NCI - MS, GC - MS/MS	Organochlorine and pyrethroids	0.02 - 4.5 $\mu\text{g}/\text{kg}$ , 0.1 - 5.0 $\mu\text{g}/\text{kg}$

### 1.3 Surface-enhanced Raman spectroscopy (SERS) for pesticide detection

Surface-enhanced Raman spectroscopy (SERS) is an ultrasensitive vibrational spectroscopy using a phenomenon of metal nanoparticles (MNPs) called “localized surface plasmon resonance (LSPR)” to enhance the Raman signal of molecules adsorbed on a surface of MNPs, which the detection limit can be down to single molecule detection. Furthermore, the SERS technique is capable to identify many compounds in the mixture without any separation like a molecular fingerprinting analysis. In the recent years, many kinds of pesticide residue can be detected with

high adsorption affinity of target molecule on metallic nanostructure. For examples, Sa'nchez-Corte's and co-workers used surface-enhanced infrared (SEIR) and surface-enhanced Raman scattering (SERS) spectroscopies to study the adsorption of dimethyl- dithiocarbamate derivative fungicides thiram and ziram on Au films [10]. Zhang *et al.* introduced the self-assembled protocol to fabricate AgNPs monolayer film as SERS Substrate for methyl-parathion detection and its detection limit can be attained at  $10^{-7}$  M [11]. Vongsvivut *et al.* demonstrated the application of SERS technique for trace detection of fonofos pesticide adsorbed on silver and gold nanoparticles [12]. Tang *et al.* applied SERS to develop a simple, sensitive, rapid and portable method for the determination of tricyclazole content in paddy rice. Its limit of detection is low as 0.002 ppm [13]. Liu and co-workers employed SERS with gold nanostructure to characterize and monitor pesticides (carbaryl, phosmet and azinphos-methyl) extracted from fruit surface. The detection limits from their fabricated nanostructure are 4.51, 6.51 and 6.66 ppm for carbaryl, phosmet and azinphos-methyl, respectively. Fan *et al.* analyzed the amount of phosmet residue in apples by SERS measurement with limit of detection around 1.01 ppm in standard solution and 1 mg/g in apple extract [14]. With many limitations of detection using conventional method, SERS technique is a great alternative for pesticide analysis.

Table 1.2 SERS technique for pesticide detection

Year	Researchers	Technique	Type of pesticide	Detection limit
2001	Sa'nchez-Corte's <i>et al.</i>	SEIR-SERS (gold film)	Dithiocarbamate (thiram - ziram)	-
2002	Kang <i>et al.</i>	SERS (silver sol)	Dithiocarbamate (thiram)	-
2011	Tang <i>et al.</i>	SERS (AgNPs)	Mixed pesticide (tricyclazole, paraquat and flusilazole)	0.01 ppm, 0.1 ppm, 2.85 ppm
2013	Liu <i>et al.</i>	SERS (AuNPs)	Organophosphate (carbaryl, phosmet and azinphos- methyl)	4.51 ppm, 6.51 ppm, 6.66 ppm (apple) 5.35 ppm, 2.91 ppm, 2.94 ppm (tomato)
2014	Yang <i>et al.</i>	SERS (Ag nanoshell)	Dithiocarbamate (thiram)	-
2014	Fan <i>et al.</i>	SERS (Au-coated substrates)	Organophosphate (phosmet)	1.01 ppm (standard solution) 1.44 mg/kg (apple)

#### 1.4 The objectives

The objectives of this research are to design and develop a high sensitive and selective detection method of carbofuran by using coupling reaction of diazonium ion combined with SERS technique.

### 1.5 Scopes of this research

1. The target pesticide of our proposed protocol is carbofuran.
2. Silver colloid used as SERS substrate is synthesized by chemical reduction method.
3. The SERS spectra of chemical interaction between azo compound from various concentrations of carbofuran and the surface of silver nanoparticles are investigated.
4. The amount of carbofuran spiked on the agricultural products is quantified using this proposed method.



## CHAPTER 2

### THEORETICAL BACKGROUND

#### 2.1 Raman spectroscopy

Raman spectroscopy is a vibrational spectroscopy to provide a chemical fingerprint of target molecule. As the vibrational spectroscopy similar to infrared (IR) spectroscopy, whereas IR bands are originated from a change in the dipole moment of a molecule but Raman bands are originated from a change in the polarizability of the molecule due to the deformation of molecule in the electric field.

When light interacts with the target molecule, some photons are adsorbed, transmitted and scattered. The light scattering includes Rayleigh scattering (elastic scattering) and Raman scattering (inelastic scattering). For Rayleigh scattering, the frequency of scattered light is equal to the frequency of incident light ( $\nu_0$ ) as shown in Figure 2.1. In Raman scattering, the frequency of scattered light is decreased to  $\nu_0 - \nu_1$ . This interaction is called Stokes scattering, Figure 2.1 (a). With excessive energy, the photons in the excited state adsorb the incident light with frequency  $\nu_0$ . Then, the frequency of scattered light with frequency  $\nu_0 + \nu_1$  is released. This is called Anti-stokes scattering, Figure 2.1 (b). For inelastic scattering, the Anti-Stoke effect is much less than the Stoke effect. Thus, the more intense Stoke effect is usually detected in Raman spectroscopy. To determine the vibrational energy levels in molecules, the different energy between ground state and excited state or Raman shift in wave numbers is calculated by equation 1.

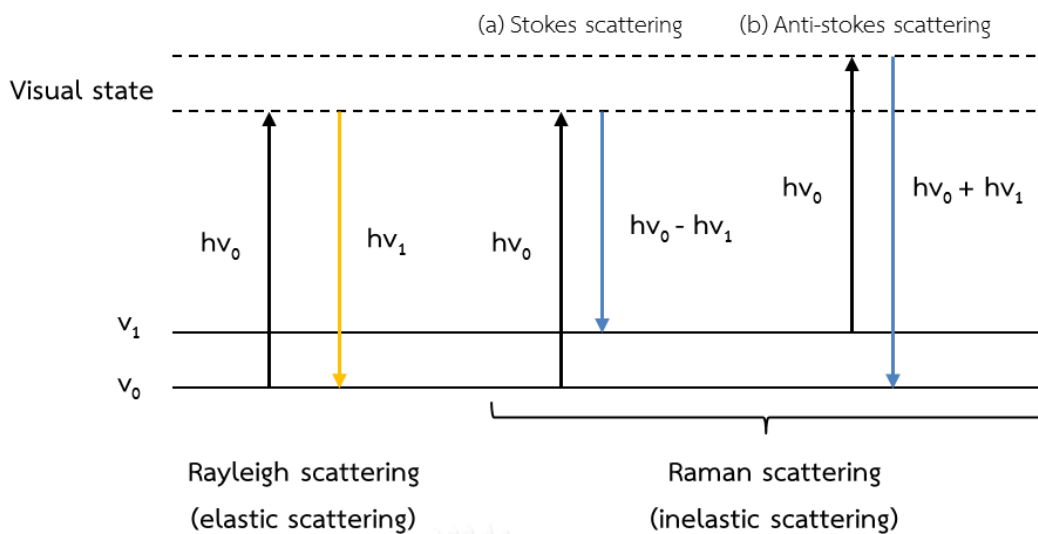


Figure 2.1 Scheme of Rayleigh scattering and Raman scattering including (a) Stoke scattering and (b) Anti-Stoke scattering.

$$\bar{\nu} = \frac{1}{\lambda_{\text{incident}}} - \frac{1}{\lambda_{\text{scattered}}} \quad (1)$$

$\bar{\nu}$  = Raman shift,  $\text{cm}^{-1}$   
 $\lambda_{\text{incident}}$  = the frequency of incident light, nm  
 $\lambda_{\text{scattered}}$  = the frequency of scattered light, nm

Generally, more than 99% of light scattering is Rayleigh scattering which is useless for molecular characterization. For this phenomenon, the Raman signal is very weak as it comes with less than 1% of the used incident light. In the experiment, it has to be measured and distinguished from the Rayleigh scattered signal [15-18].

## 2.2 Localized surface plasmon resonance (LSPR)

As the particle size of nanostructure between 1–100 nm, the formation of fascinating material properties with uncommon characteristics, which cannot be observed in the larger materials, is dramatically occurred including mechanical,

electrical, thermal, chemical and optical properties. These are attentively considered hereby as metallic nanoparticles (NPs).

To consider the phenomenon of their unique optical properties, surface plasmons (SPs) are involved with delocalized electron oscillation at the interface of metal-dielectric interface. The charge motion of oscillating electrons can always generate the electromagnetic field, which is called surface plasmon polariton, as shown in Figure 2.2 (a). For the close surface of small particles, it is called localized surface plasmon. According to the size of metal nanoparticles, which is smaller than the wavelength of incident light, the frequency of incident photon possibly matches the natural frequency of electron oscillating on the surface of NPs. This induces the phenomenon called “Localized surface plasmon resonance (LSPR)” which can be locally occurred around the NPs as shown in Figure 2.2 (b) [19]. Because of the strong enhancement of surface electric field, many investigations are possible to use Raman spectroscopy combined with LSPR from metal nanoparticles to enhance the Raman signals in the level of  $10-10^8$  times compared with the normal Raman signals. These techniques including surface-enhanced Raman spectroscopy (SERS) [10, 12, 13], surface-enhanced fluorescence spectroscopy (SPFS) [20, 21], refractive index (RI) measurement [22], biomolecular interaction detection [23], surface-enhanced infrared adsorption spectroscopy (SEIRA) [24, 25] are widely used across the world.

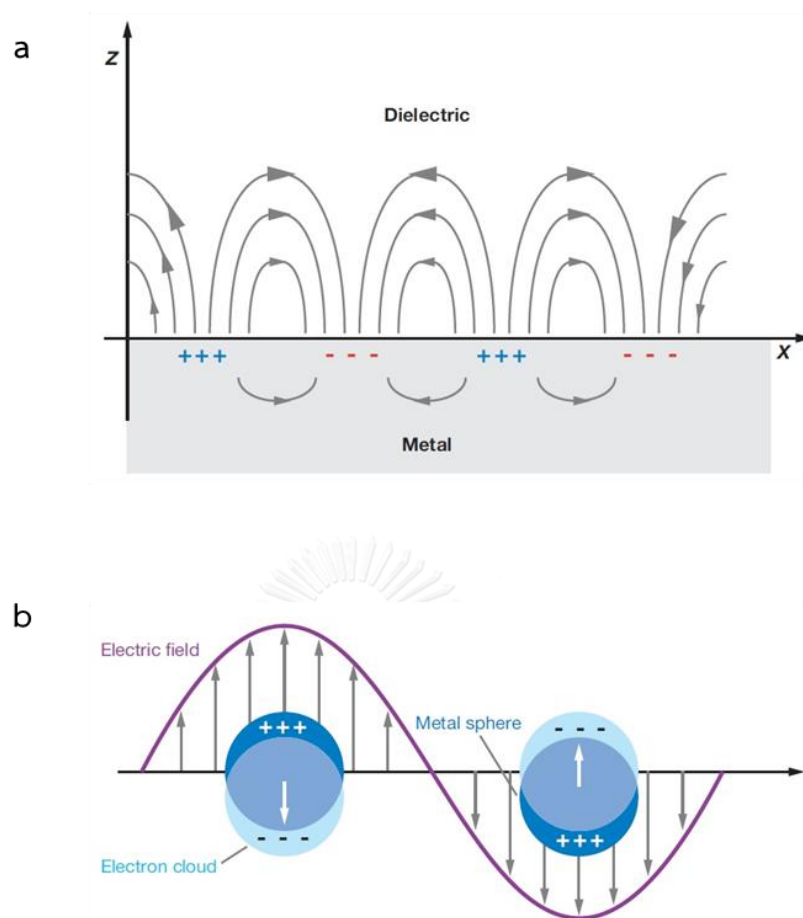


Figure 2.2 Schemes of (a) a surface plasmon polariton for planar interface and (b) a localized surface plasmon for nanoparticles [19]

### 2.3 Surface-enhanced Raman spectroscopy (SERS)

Currently, the recent advance in the fabrication and chemical engineering of metal colloid offer a great opportunity in the development of SERS detection approach with high sensitivity and selectivity. Several non-functionalized target analytes can be detected in ultrasensitive level by simply depositing the analyte on the surface of metal nanoparticles (MNPs) such as gold nanoparticles (AuNPs), silver nanoparticles (AgNPs) *etc.* These metal nanostructures can generate surface plasmon polarization from the electron oscillating on a metal surface. This produces intense electromagnetic fields up to  $10^8$  times. This phenomenon leads to the enhancement capability of Raman measurement when the target molecules are in a “hot spot” of



aggregated nanoparticles. The enhanced fingerprint Raman spectrum of the target analyte at trace concentration is measured and collected *via* the capability of strong localized surface plasmon resonances (LSPR) in the hot spot [12, 13, 16, 26]. Hence, the close contact of target molecules with the metallic surface is critically required (typically less than 10 nm) [15].

## 2.4 Hydrolysis of carbofuran

In the environment, the degradation of carbofuran naturally occurs by the combination of two main processes which are chemical hydrolysis and microbial degradation influenced by environmental properties including moisture contents, pH and organic molecules (Table 2.1).

Table 2.1 Half-life of carbofuran in degradation process

Degradation process	Half-life (days)	Environmental conditions
Hydrolysis	27.7	pH 7, 25 °C
	2.73	pH 8, 25 °C
	0.54	pH9, 25 °C
Aqueous photolysis	$7.95 \times 10^3$	pH 7, 28 C
Soil photolysis	138	pH 5.7, 27 °C, sandy loam, 2.1% organic molecule, 21% moisture
Aerobic biodegradation	22.0	pH 5.7, 25 °C, sandy loam, 2.1% organic molecule, 21% moisture
Anaerobic biodegradation	30.0	pH 5.7, 25 °C, sandy loam, 2.1% organic molecule, 21% moisture
Field dissipation	13.0	pH 7.3, sandy loam, 0.38% organic molecule

Carbofuran as a systemic methylcarbamate has a long half-life because it is very stable in acidic and neutral medium, but will be hydrolyzed in alkaline condition. As a primary degradation, chemical hydrolysis is much quicker under alkaline condition [27-31]. For base-catalyzed hydrolysis, carbofuran phenol is the main compound from the degradation process of carbofuran in water and solid as shown in Figure 2.3 [32-35]. From the degradation process of carbofuran, other products are possibly generated including 3-hydroxy carbofuran, 3-hydroxy carbofuran-7-phenol, 3-keto carbofuran and 3-keto carbofuran-7-phenol [36].

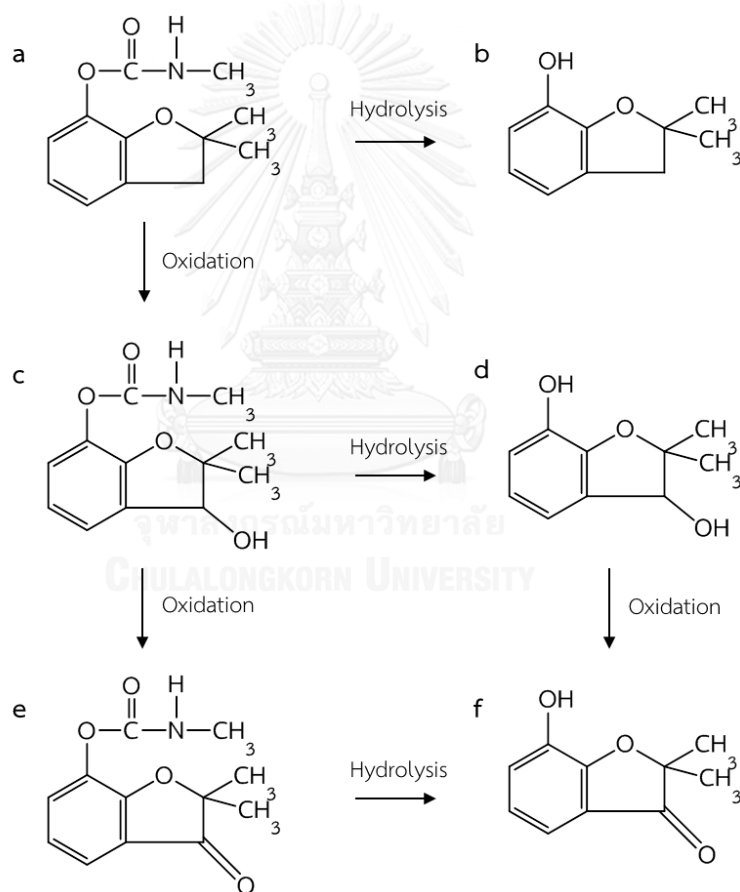


Figure 2.3 Scheme of degradation process of carbofuran ; (a) carbofuran, (b) carbofuran phenol, (c) 3-hydroxy carbofuran, (d) 3-hydroxy carbofuran-7-phenol, (e) 3-keto carbofuran and (f) 3-keto carbofuran-7-phenol.

In 1978, Seiber and co-workers studied the hydrolysis reaction of carbofuran in rice paddy water and deionized (DI) water. They reported that half-lives at pH 7 and 10 were 864 hours and 1.2 hours, respectively. It indicated that the alkali-catalyzed hydrolysis of carbofuran at pH 10 was more than 700 times quicker than at pH 7 [33].

In 1996, Bailey *et al.* found that the hydrolysis rate of carbofuran dramatically increased with an increase of pH. At pH 3 and 25 °C, 80–95% of the amount of carbofuran spiked after 1, 3, and 6 hours was recovered. On the other hand, only 65% of the initial amount at pH 10 was recovered after 1 hour, 35% kept after 3 hours and 10% kept after 6 hours [37].

For this reason, the alkali-catalyzed hydrolysis is essentially step to originate carbofuran phenol as a major product from carbofuran. Therefore, amount of carbofuran can be directly quantified from the carbofuran phenol which is used in coupling reaction which is detailed described in the next section.

## 2.5 Azo coupling reaction

Azo coupling reaction is the most popular organic reaction between diazonium ions and strongly activated aromatic compound such as anilines or phenols in the formation of aryl azo compound (Figure 2.4). In this electrophilic aromatic substitution, the diazonium cation is the electrophile and the activated aromatic compound is a nucleophile. The substitution usually occurs at the *para*-position, except that this position is occupied. In which case, the *ortho*-position is preferred as shown in Figure 2.5. The pH of solution is carefully considered because the reaction cannot occur in strong acidic solution.

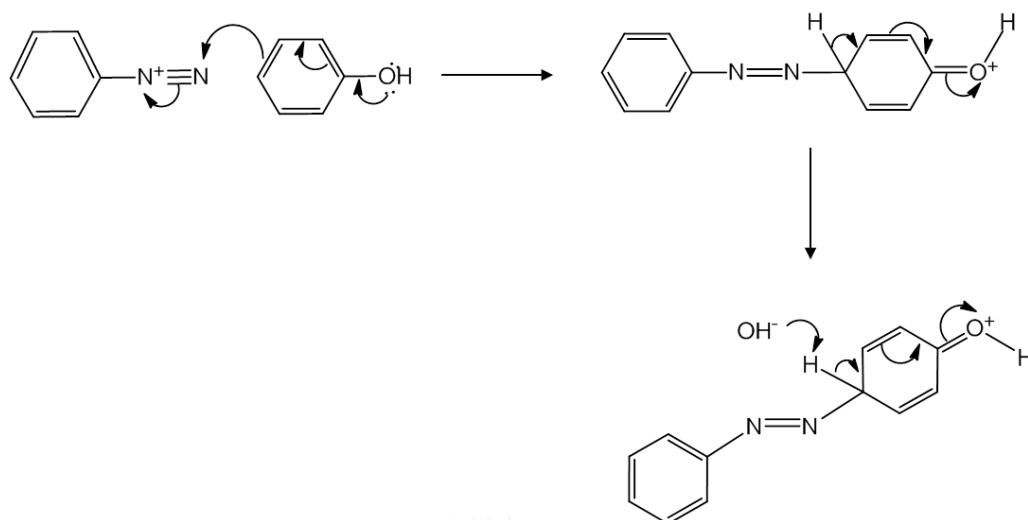


Figure 2.4 Mechanism of coupling reaction for the formation of aryl azo compound.

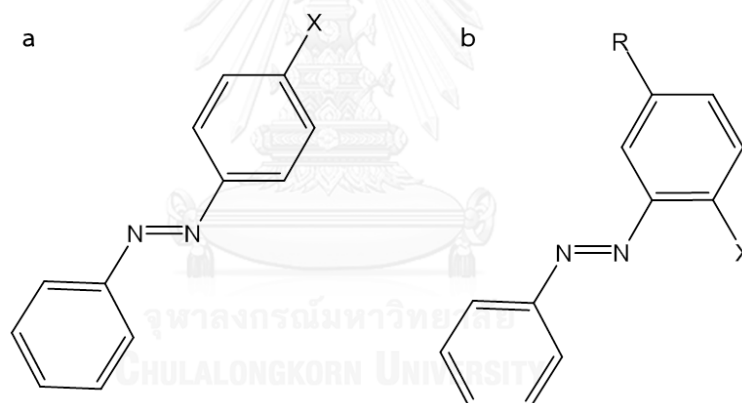


Figure 2.5 Structure of aromatic azo compound at (a) *para*-, (b) *ortho*-position ; where X is  $\text{-NH}_2$  or  $\text{-OH}$  group and R can be both alkyl and aryl group.

As an important intermediate in this reaction, aromatic diazonium ion ( $\text{Ph-N}^+\equiv\text{N}$ ) is prepared by the treatment of aromatic amines with nitrous acid. This is called diazotization (Figure 2.6). Generally, nitrous acid is produced from sodium nitrite and inorganic acid at low temperature ( $0\text{--}5\text{ }^\circ\text{C}$ ). Because aryl diazonium salt is very unstable at temperature above  $5\text{ }^\circ\text{C}$ ,  $\text{-N}^+\equiv\text{N}$  group can decompose to form  $\text{N}_2$  (nitrogen gas). So the azo coupling reaction is typically conducted in near freezing point. The color of azo compound is primarily in the yellow to red. Due to the

extended conjugated system of aromatic azo compound, it can adsorb long wavelength of light especially that is in the visible regions. In common, azo compound is widely used as the dye and pigment in the industry such as textile, biomedical investigation and organic synthesis in scientific research [38-40].

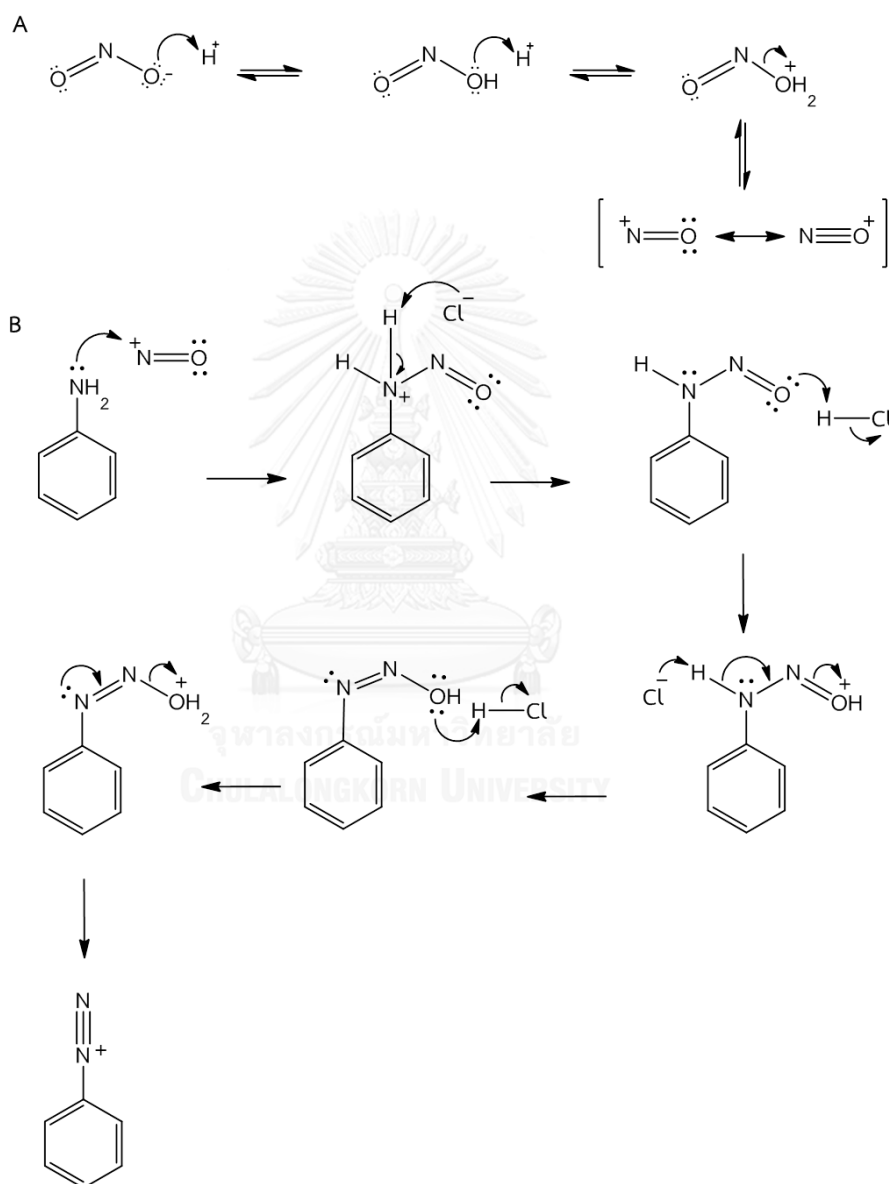


Figure 2.6 Mechanism of diazotization for the formation of diazonium ion

## CHAPTER 3

### EXPERIMENTS

#### 3.1 Chemicals and instruments

- Silver nitrates ( $\text{AgNO}_3$ ) (Carlo Erba reagents S.A.S.)
- Tri-sodium citrate ( $\text{Na}_3\text{C}_6\text{H}_5\text{O}_7$ ) (Carlo Erba reagents S.A.S.)
- Potassium hydroxide (KOH) (Carlo Erba reagents S.A.S.)
- Sodium nitrite ( $\text{NaNO}_2$ ) (Carlo Erba reagents S.A.S.)
- Carbofuran ( $\text{C}_{12}\text{H}_{15}\text{NO}_3$ ) (Sigma-Aldrich Co. LLC.)
- 4-aminothiophenol (4-ATP,  $\text{C}_6\text{H}_7\text{NS}$ ) (Sigma-Aldrich Co. LLC.)
- Concentrated hydrochloric acid (HCl) (Merck Sharp & Dohme Corp.)
- Absolute ethanol ( $\text{C}_2\text{H}_6\text{O}$ ) (Merck Sharp & Dohme Corp.)

All chemicals were analytical reagent grade and were used as received without prior purification. In order to prepare the analyte solution, ethanol was used to dissolve Carbofuran, KOH and 4-ATP, while the other chemicals were dissolved in deionized (DI) water.

UV-visible spectra were utilized by Ocean Optics USB4000 Fiber Optic Spectrometer coupled with a DH-2000 deuterium light source from Mikropack.

#### 3.2 The synthesis of silver nanoparticles (AgNPs)

As the mainstream protocol [41], AgNPs colloid was prepared by the reduction of  $\text{AgNO}_3$  with  $\text{Na}_3\text{C}_6\text{H}_5\text{O}_7$ . To prepare AgNPs solution, 200 mL of 1 mM  $\text{AgNO}_3$  solution was heated until its boiling for 5 minutes. Then, 4 mL of 1%  $\text{Na}_3\text{C}_6\text{H}_5\text{O}_7$  solution was added to the boiled  $\text{AgNO}_3$  solution under a vigorous stir. The mixed solution was kept boiling and stirring energetically for 30 minutes. Milky brown AgNPs solution was characterized by UV-visible adsorption spectroscopy.

### 3.3 The alkaline hydrolysis reaction of carbofuran

To increase the selectivity of SERS measurement, a target compound with a derivative phenol as a functional group is required. In the case, a target pesticide, which is carbofuran, was chemically transformed into carbofuran phenol by a following protocol. For the formation of carbofuran phenol, carbofuran was hydrolyzed in alkaline solution by mixing 49.5 mL of carbofuran in ethanol with 0.5 mL of 20 M KOH. After mixing, the solution was heated at 50 °C for 3 hours. After hydrolysis, the solution was cooled down to 0 °C by using ice-bath for following investigation. The scheme of the hydrolysis reaction is demonstrated in Figure 3.1.

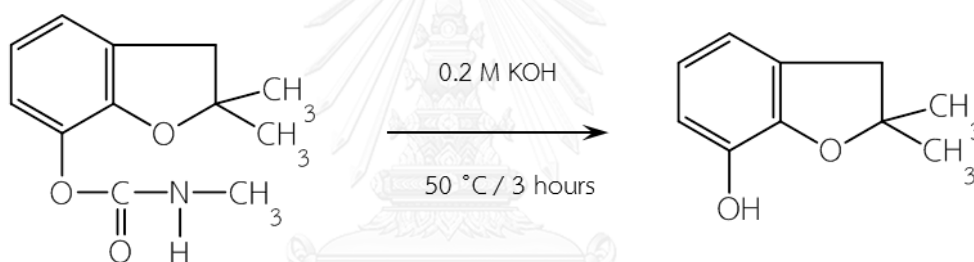


Figure 3.1 The alkaline hydrolysis reaction of carbofuran for generating carbofuran phenol.

### 3.4 The preparation of azo compound using coupling reaction

In the diazotization, diazonium ion was generated by mixing 1 mM 4-ATP in 0.1 M HCl with 5% NaNO<sub>2</sub> solution (1:1, v/v, 725 eq) at 0 °C for a minute (Figure 3.2 (a)). The azo-coupling reaction was achieved by adding the prepared carbofuran phenol from alkaline hydrolysis into the mixture (1:1, v/v) as shown in Figure 3.2 (b). After mixing, the solution was incubated to complete a chemical reaction at 0 °C for a minute. Then, the solution was kept in hot water-bath at 50 °C for 15 minutes in order to eliminate the excess diazonium ions.

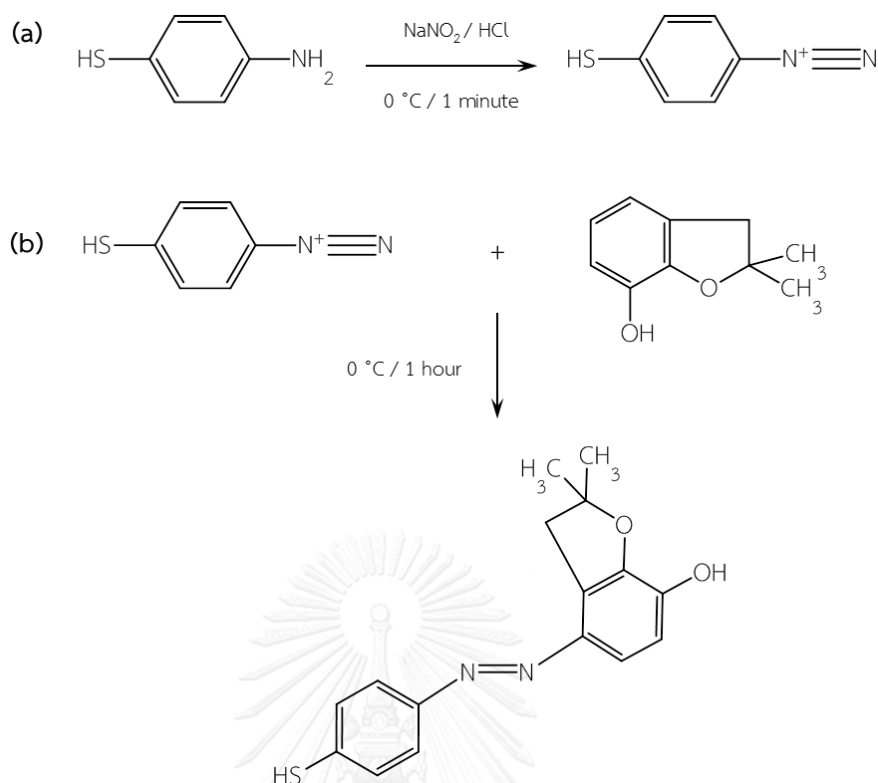


Figure 3.2 (a) The diazotization for preparing diazonium ion and (b) The diazo coupling reaction for generating the azo compound.

### 3.5 SERS measurement

To carry out the SERS measurement, SERS spectra were measured using DXR Raman microscope (Thermo scientific) with a 780-nm as an excitation laser. Each sample was analyzed under a 10X-objective lens with a laser spot size 3.1  $\mu\text{m}$ . To receive the Raman spectra, the typical laser power used was 14 mW with an aperture at 50  $\mu\text{m}$  slit and the exposure time for measuring is 2 seconds with 8 accumulations. After azo-coupling reaction, each sample was mixed with silver colloid in the volume ratio of 1 to 1 for 5 minutes. The mixture was dropped on an aluminum plate. SERS spectra were collected using 2-s exposure time with 8 accumulations. All spectra were presented without any correction.



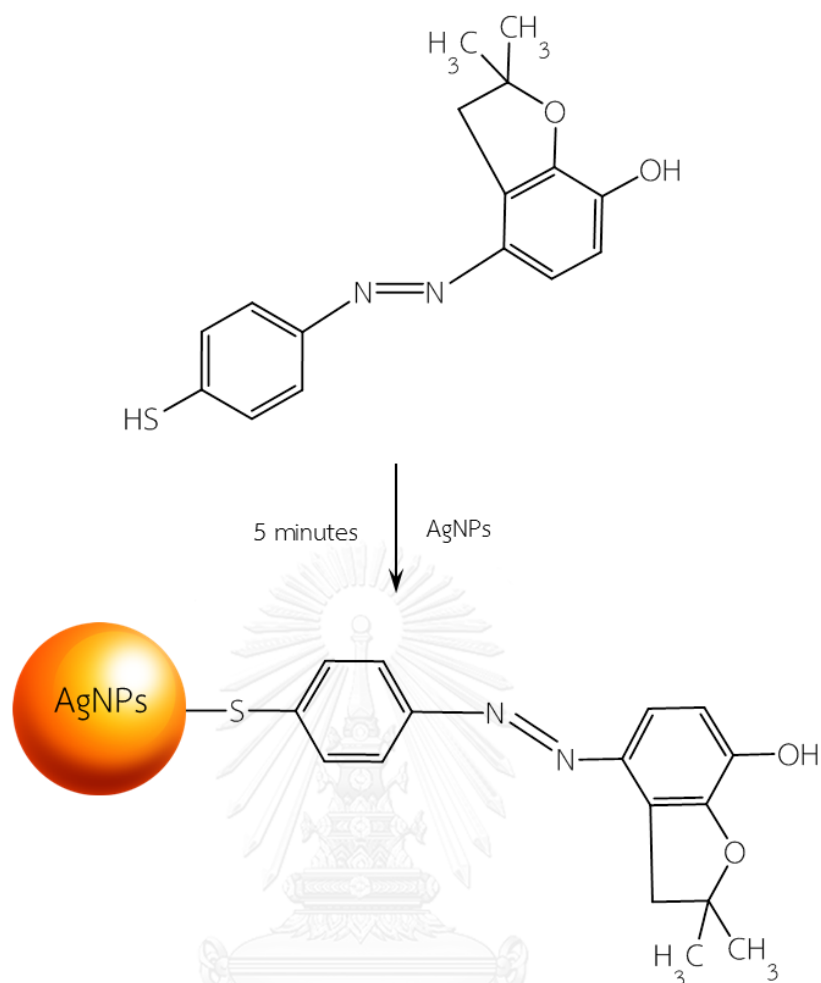


Figure 3.3 The deposition of azo compound on the surface of AgNPs.

### 3.6 Effect of interfering substances on the detection method

Under consideration of interference, e.g. acetic acid, ascorbic acid, formic acid, fructose, glucose, lactose, maltose, NaCl and table sugar, 5 ppm carbofuran in the solution of 1mM interfering substances was incubated in 0.2 M KOH solution at 50 °C for 3 hours. After hydrolysis reaction, the solution was kept under 0–5 °C until further investigation. Before coupling reaction, 1 mM 4-ATP in acidic solution at freezing point was mixed together with 5% NaNO<sub>2</sub> solution (1:1, v/v) for one minute to prepare diazonium ion. Then, the solution of 5 ppm carbofuran phenol was added into the solution of diazonium. The temperature of mixture remained at the freezing point for a minute. Finally, the solution of azo compound was warm in water-bath at 50 °C for 15 minutes. For SERS measurement, the mixture between azo compound

and silver colloid was incubated at room temperature for 5 minutes and detected by Raman spectroscopy.

### 3.7 Method validation of carbofuran detection in real samples

To investigate the validation of our proposed method, 0.1–5 ppm carbofuran were spiked in 5 grams of each sample such as rice, soya bean, white pepper, black pepper, mung bean, sesame, peanut and chili pepper. Next, the total amounts of carbofuran on sample surface were removed by 5 mL of ethanol. In alkali-catalyzed hydrolysis, carbofuran residues from each sample were hydrolyzed in the solution of 0.2 M KOH at 50 °C for 3 hours. For diazotization, 1 mM 4-ATP in acidic solution at freezing point was added into 5% NaNO<sub>2</sub> solution (1:1, v/v) for one minute. Then, the solution of carbofuran phenol formed by alkaline hydrolysis was mixed together the solution of diazonium ion to generate orange azo compound under 0–5 °C. To eliminate excess diazonium ion completely, the mixture was heated in hot water-bath at 50 °C for 15 minutes. As SERS technique, SERS spectra of 0.1–5 ppm carbofuran from each sample were collected by analyzing the mixture of azo compound and silver colloid *via* Raman spectroscopy.

## CHAPTER 4

### RESULTS AND DISCUSSION

#### 4.1 The synthesis of colloidal citrate-reduced silver nanoparticles

AgNPs was synthesized *via* the reduction of  $\text{AgNO}_3$  with trisodium citrate ( $\text{Na}_3\text{C}_6\text{H}_5\text{O}_7$ ) using Lee-Meisel method[42], which  $\text{Na}_3\text{C}_6\text{H}_5\text{O}_7$  acts as both reducing agent and stabilizer. After adding reducing agent into the solution of  $\text{AgNO}_3$ , the color of mixture slowly changed from colorless to milky yellow brown (see an inset of Figure 4.1). The plasmonic extinction spectrum of synthesized AgNPs was collected using UV-visible spectroscopy and shown in Figure 4.1. The in-plane dipole plasmon resonance of AgNPs appears at at  $\sim 430$  nm, which suggests the average particle size of  $\sim 50$  nm. The quadrupole plasmon resonance can also be observed as a shoulder at 350 nm in a spectrum indicating the formation of large particles. The broad peak at 430 nm with a very high full width at half maximum also implies a broad distribution of particle size.

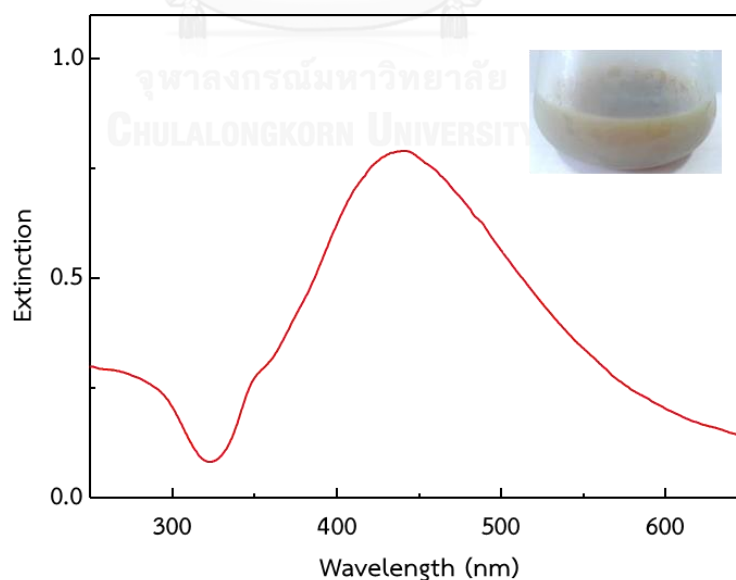


Figure 4.1 Plasmonic extinction spectrum of synthesized colloidal AgNPs.

## 4.2 The interaction between carbofuran and AgNPs

In this part, carbofuran was qualitatively investigated by direct SERS detection. The solution of carbofuran was mixed together with silver colloid. The mixture was further stirred to ensure that it was homogenous and AgNPs were completely aggregated. Then, SERS spectrum of the prepared mixture was collected. SERS spectra collected from AgNPs dispersed in 1000 ppm carbofuran and in ethanol, which is a solvent for carbofuran, are shown in Figure 4.2. The two spectra in Figure 4.2 are identical. The peaks at 1454 and 2800–3000, 1277, 1086 and 1048, and 879  $\text{cm}^{-1}$  are attributed to C-H stretching,  $\text{CH}_2$  bending, C-O stretching, and C-C stretching, respectively [43, 44]. These Raman signals represent the characteristic vibration modes of ethanol which was used as solvent. This observation indicates that carbofuran cannot be directly detected by SERS technique because carbofuran molecules might not be adsorbed directly on the surface of citrate-coated AgNPs [45]. According to low chemical affinity and steric hindrance for physical adsorption of citrate-coated AgNPs [46, 47], no adsorption of carbofuran can occur. As a result, this research completely required the others method to increase more affinity of carbofuran with the metal surface for good SERS measurement.

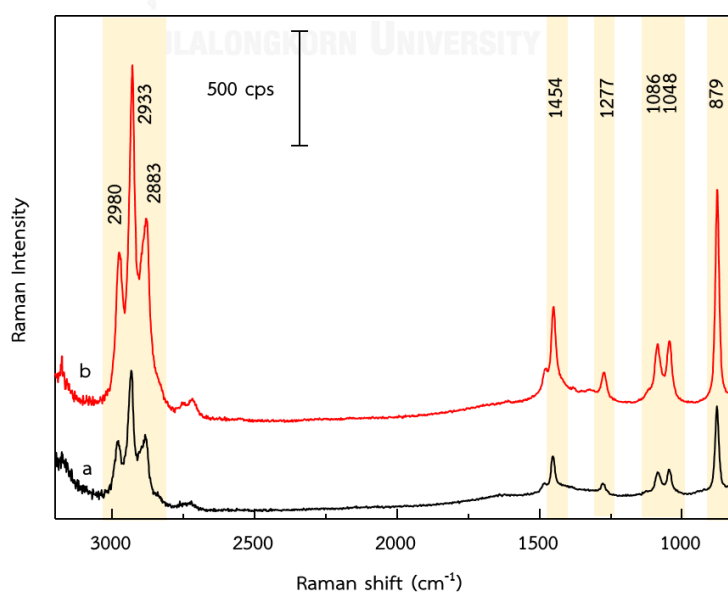


Figure 4.2 SERS spectra of (a) ethanol and (b) 1000 ppm carbofuran in ethanol.

### 4.3 The formation of azo compound

As we already mentioned earlier in section 4.2 that molecules of carbofuran might not be adsorbed well on the metal surface, it cannot be directly measured by SERS technique. It is quite well-known that silver metal can easily form Ag-S bond with thiol molecule [17, 48]. To enhance the adsorption affinity of carbofuran on the metal surface, a functional group with an -SH (thiol) group need to be added on a molecule of carbofuran. In this study, a diazo coupling reaction is introduced. Firstly, carbofuran was hydrolyzed to carbofuran phenol. Secondly, diazonium salt solution was prepared by mixing 4-ATP in a solution of 0.1 M HCl and 5% NaNO<sub>2</sub> solution at volume ratio 1:1 (v/v). The generated carbofuran phenol will react specifically with the diazonium ion to form an azo compound. Figure 4.3 shows the overall chemical reaction to generate an azo compound with an -SH group. By these reaction, the generated azo compound with an -SH group can easily bond on a surface of AgNPs to obtain SERS signals.

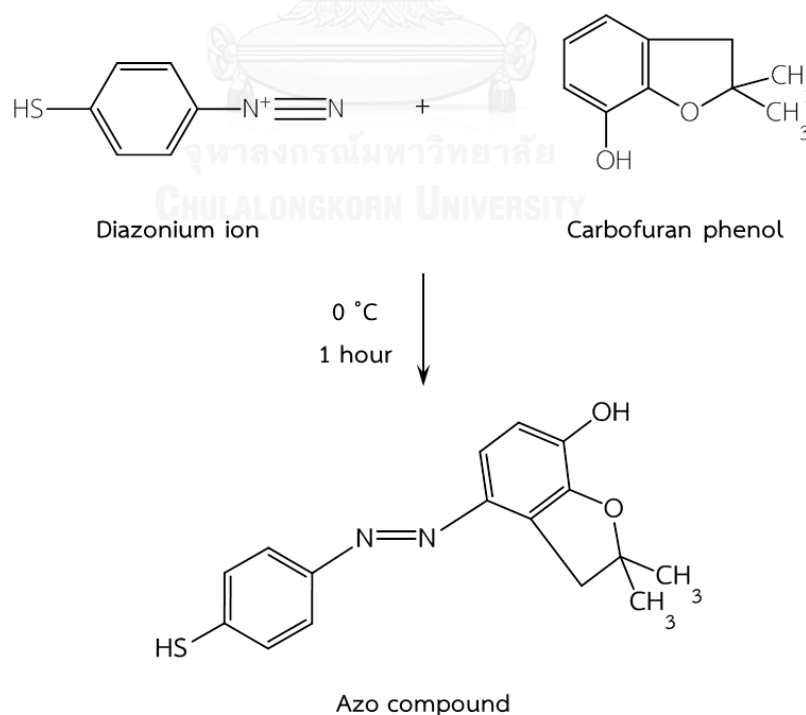


Figure 4.3 The diazo coupling reaction to produce an azo compound with -SH group from carbofuran phenol.

We assumed that the molecule of carbofuran was completely changed into carbofuran phenol as a carbofuran derivative. Therefore, the quantity of carbofuran is precisely equal to that of carbofuran phenol. To confirm the formation of azo compound, UV-vis spectra of azo compounds generated using various concentrations of carbofuran (0–1000 ppm) were collected, as shown in Figure 4.4. Without carbofuran, there is no absorption band in UV-visible spectrum. On the other hand, the mixture with 1000 ppm carbofuran shows a strong characteristic absorption band at ~480 nm, which is directly related to the whole electronic transition of a  $\pi \rightarrow \pi^*$  in -N=N- of the azo compound with charge-transfer character and originating primarily from the phenolic group [49]. The absorbance of this band decreases with a decrease in the concentration of carbofuran.

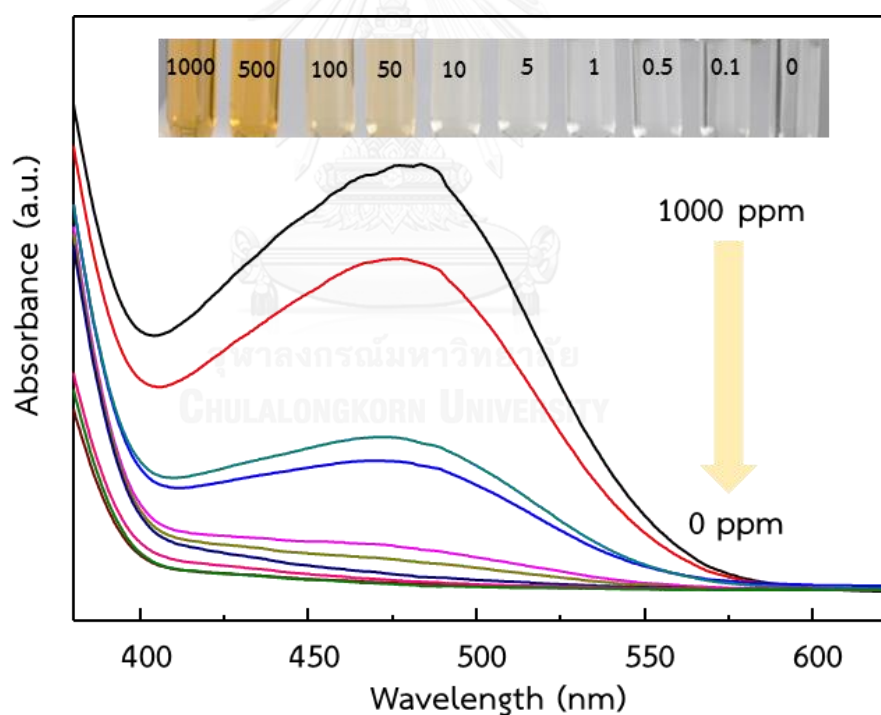


Figure 4.4 UV-visible spectra of the azo compounds generated using various carbofuran concentrations (0–1000 ppm). The inset demonstrates the corresponding solution color of azo compounds at various carbofuran concentrations.

To quantify carbofuran by using UV-visible spectroscopic technique, the absorbance at 480 nm was linearly plotted against the concentration of carbofuran ranging from 0.5–50 ppm with  $R^2 = 0.9966$  (Figure 4.5) and the limit of detection (LOD) is 18.79 ppm. As a result, the use of this UV-visible spectroscopic technique is not nearly capable to detect carbofuran at a maximum residue limit (0.1 mg/kg, 0.02 mg/kg (EU)) even though it is a selective method.

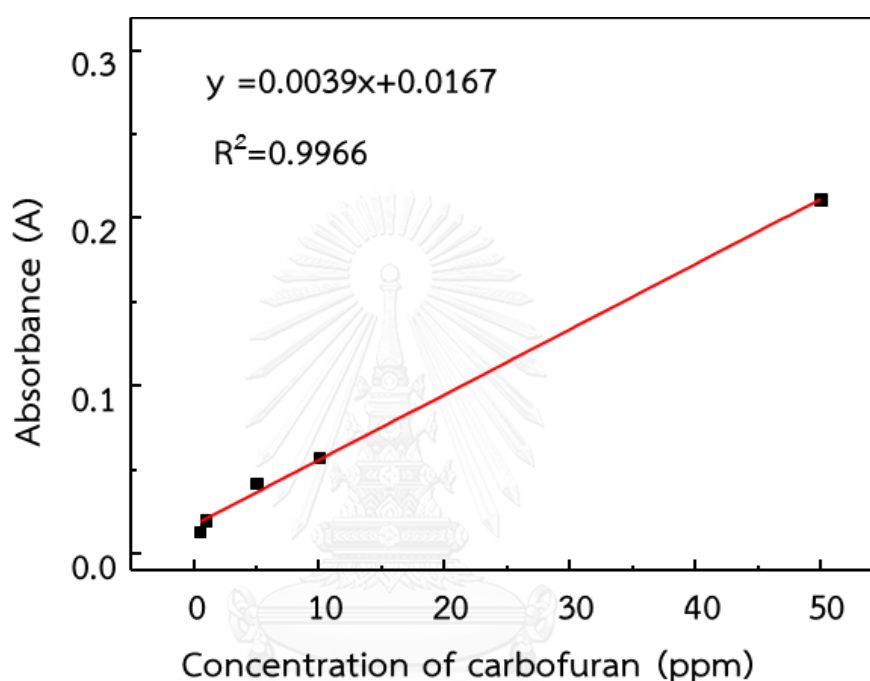


Figure 4.5 The correlation of carbofuran concentration (0.5–50 ppm) and absorbance at 480 nm.

To consider the particular activity of AgNPs *via* the behavior of electron oscillation, Figure 4.6 shows extinction spectra of AgNPs and AgNPs with azo compound. A LSPR band at around 430 nm associates with in-plane dipole oscillation of electron on the surface of AgNPs. A change in this band relates to the different frequency of electron oscillation on AgNPs surface [50]. For AgNPs with azo compound, a red shift of LSPR band to ~460 nm can be observed. It suggests that the electron oscillation on the AgNPs surface is interfered, which implies the deposition of azo compound molecules on the AgNPs surface [51, 52].

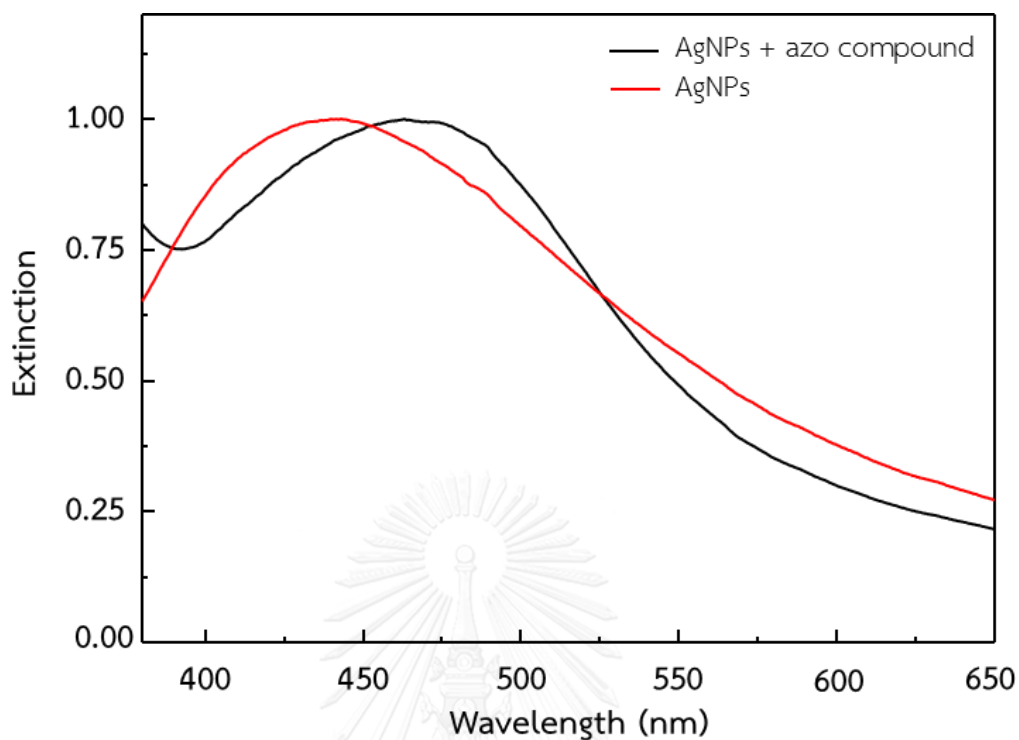


Figure 4.6 Extinction spectra of AgNPs and AgNPs with azo compound.

#### 4.4 Carbofuran detection using surface enhanced Raman scattering

To create and develop a selective and sensitive detection method, a coupling reaction was employed to produce an azo compound with thiol group as shown in previous section. The azo compound can directly attach on the AgNPs surface *via* a Ag-S bond [53], as shown in Figure 4.7.

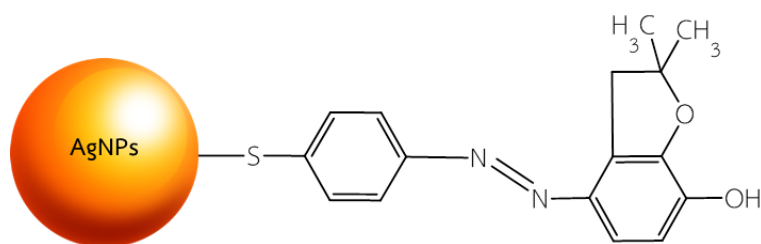


Figure 4.7 Scheme of azo compound on the surface of silver nanoparticles.



To test our hypothesis, Figure 4.8 shows SERS spectra of 1000 ppm carbofuran phenol and compounds from an azo coupling reaction using 0 and 100 ppm carbofuran. All of these samples were collected at the identical measurement conditions using AgNPs as a SERS substrate. For carbofuran phenol from alkaline hydrolysis, its SERS spectrum with very low Raman intensity was obtained. This suggests that the carbofuran phenol cannot be directly detected using SERS technique. This observation reveals that either carbofuran or its derivative (carbofuran phenol) cannot well adsorb on the metal surface reflecting on the low intensity of Raman signal. Without employing carbofuran in an azo coupling reaction, the characteristic peak of  $-N^+\equiv N$  group in the region  $2300\text{--}2130\text{ cm}^{-1}$  [54] cannot be observed because the functional group  $-N^+\equiv N$  is unstable at temperatures above  $5\text{ }^\circ\text{C}$ . It is easily to be decomposed into  $N_2$  and form  $-OH$  group (Figure 4.9). According to peaks at  $1590, 1571, 1429, 1387$  and  $1327\text{ cm}^{-1}$ , which can be observed in Figure 4.8 and are assigned as in Table 4.1, they confirm the formation of 4-mercaptophenol on the surface of AgNPs.



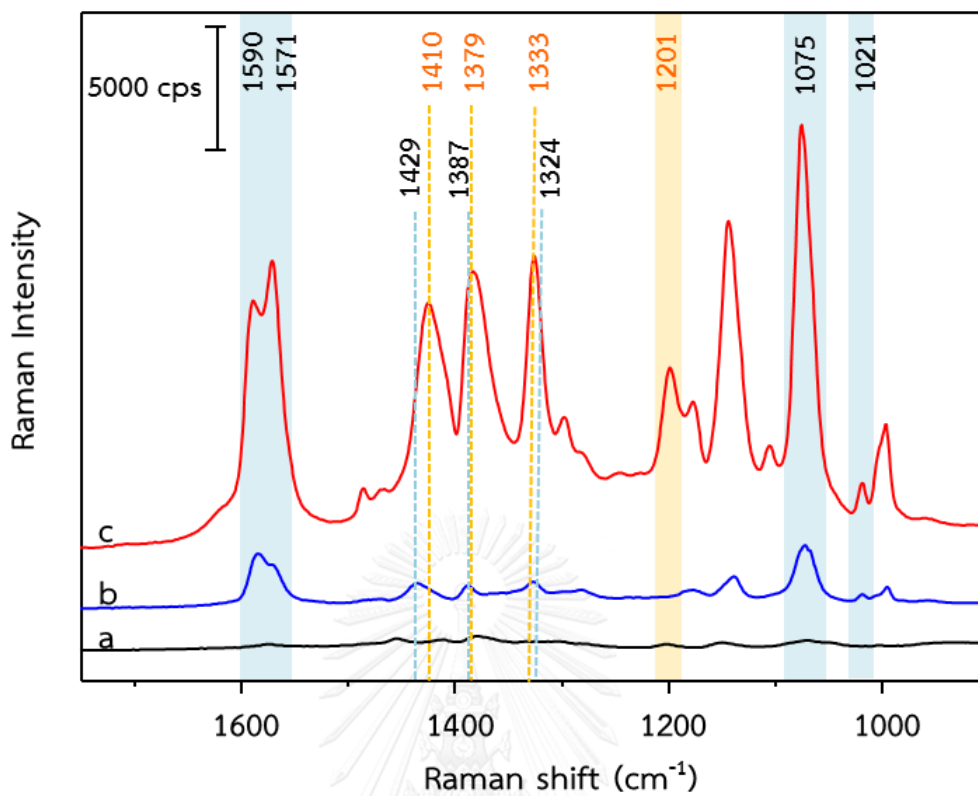


Figure 4.8 SERS spectra of (a) 1000 ppm carbofuran phenol and compounds from an azo coupling reaction using (b) 0 and (c) 100 ppm carbofuran.

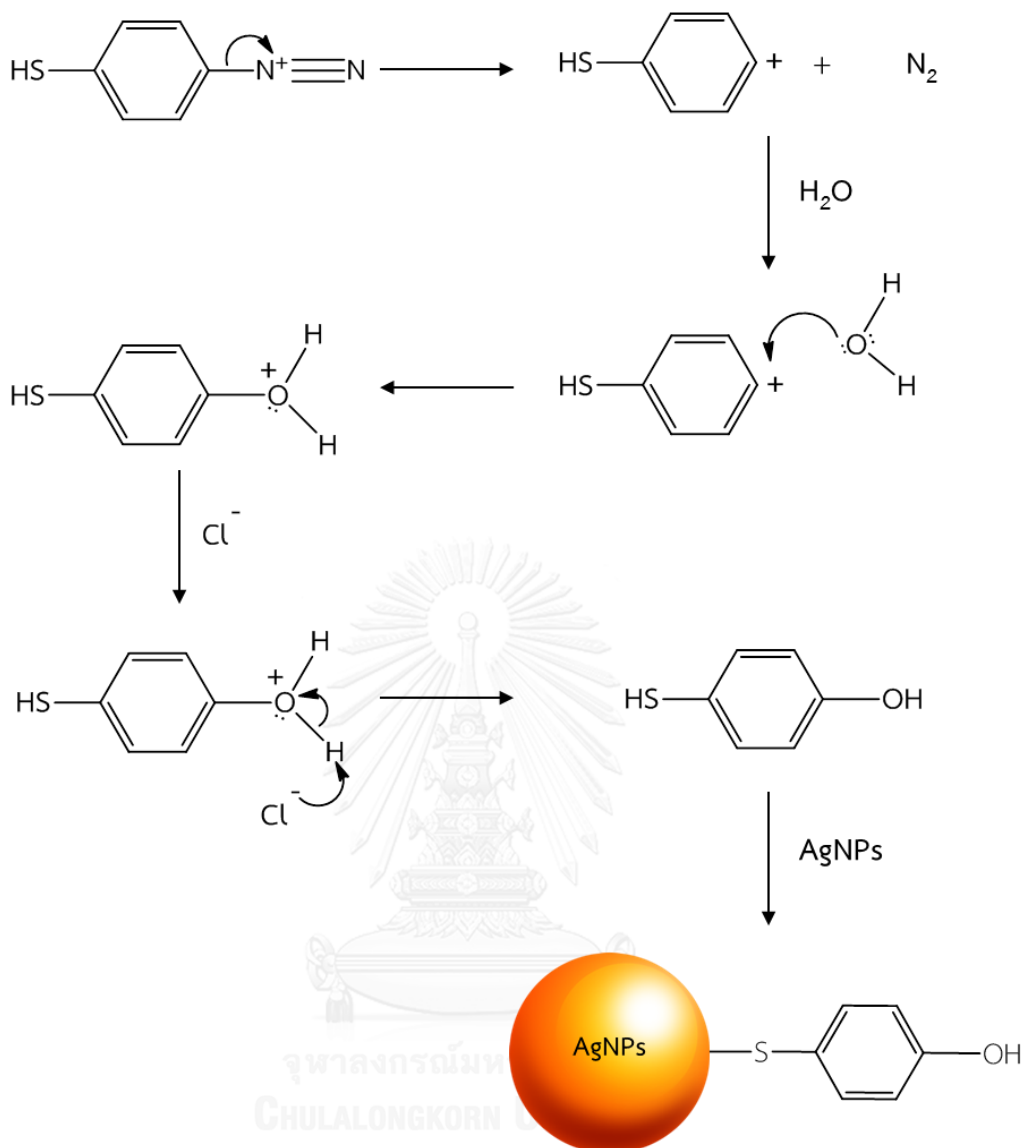


Figure 4.9 The formation mechanism of 4-mercaptophenol on the surface of AgNPs.

For an azo coupling reaction using 100 ppm carbofuran, the SERS spectrum are assigned in Table 4.1 [41]. The characteristic peak of  $\text{-N=N-}$  stretching at  $1410\text{ cm}^{-1}$  can be observed. Moreover, the peaks of phenol ring at  $1333$  and  $1379\text{ cm}^{-1}$  are slightly different from that of phenyl ring in 4-mercaptophenol indicating a structural difference in molecular environments around a phenyl ring. Also, the peak of CN stretching, CH and OH bending, CNN in plane bending and CC stretching at  $1201\text{ cm}^{-1}$  can obviously prove the chemical production of azo compound. In Figure 4.8, SERS spectrum of azo compound generated from

diazonium ion and carbofuran phenol can be achieved with high Raman intensity. A strong SERS signal at  $1075\text{ cm}^{-1}$  of C-S stretching was observed. This suggests that the C-S bond of the azo molecule is strongly attached on the surface of AgNPs *via* Ag-S bond. This phenomenon induces the azo molecule positioned in hot spots (high electric field enhancement). The adsorption efficiency affects the SERS signal and the sensitivity. These observations indicate that our synthesized azo compound is able to adsorb efficiently on the surface of silver-citrate nanoparticle which is used to provide the enhancement of Raman signal.

Table 4.1 SERS Peak Assignments for 4-mercaptophenol and azo compound

Raman shift ( $\text{cm}^{-1}$ )		SERS assignment
4-mercaptophenol	Azo compound	
1021	1021	Aromatic =C-H in plane formation
1075	1075	C-S stretching
	1201	C-N stretching, CNN (phenyl-N) in plane bending, C-H and O-H bending, C-C stretching from phenol group
1327		CCH bending
	1333	NCC bending with phenyl rings
1387	1379	C-C stretching with phenyl rings; C-H and O-H bending from phenol group
	1410	-N=N- stretching
1429		C-H and O-H bending from phenol group
1571	1571	
1590	1590	C-C stretching within phenol

#### 4.5 Effect of incubation time in alkaline hydrolysis reaction

As a natural chemical process, alkali-catalyzed hydrolysis of carbofuran is a major degradation process to generate carbofuran phenol (Figure 4.10) [28-31, 55]. To promote the formation of azo compound in this procedure, the incubation time of

carbofuran hydrolysis is certainly in a critical condition. The incubation time was varied in the range of 0–180 minutes.

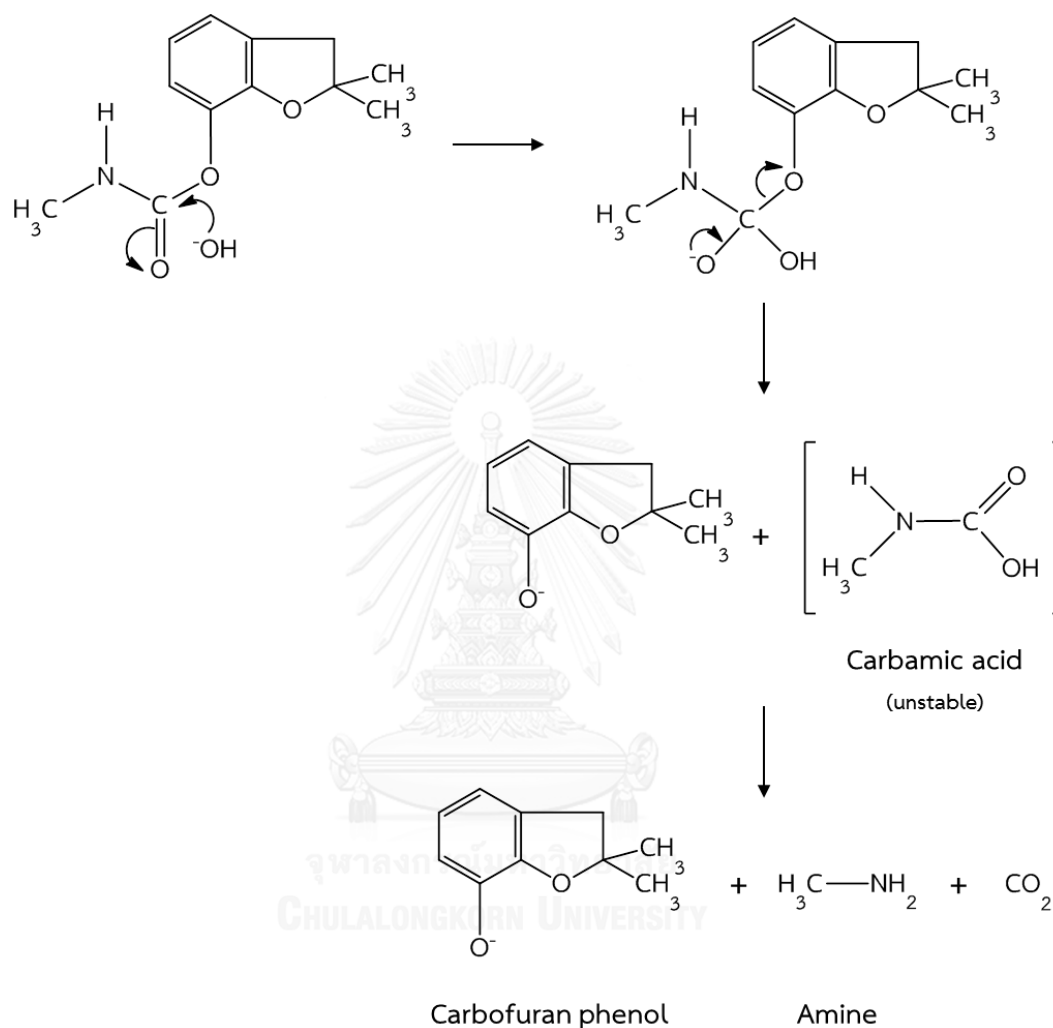


Figure 4.10 Alkali-catalyzed hydrolysis mechanism of carbofuran to carbofuran phenol.

In this observation, the vibrational peak position of azo compound at  $1201\text{ cm}^{-1}$  is specifically considered because it is an obvious characteristic band of azo compound from carbofuran derivative. Figure 4.11 shows the Raman intensity of azo compound at  $1201\text{ cm}^{-1}$  with various incubation time of alkaline hydrolysis reaction. The standard deviations of each sample are 364.15, 513.06, 387.86, and

320.54 for 0, 60, 120, and 180 minutes, respectively. As a result, the Raman intensity increases with an increase in hydrolysis time (~1900 to ~4000 cps). To prepare the azo compound from the total amount of carbofuran phenol as much as possible, the incubation time of hydrolysis at 3 hours is chosen due to the highest intensity and the least standard deviation.

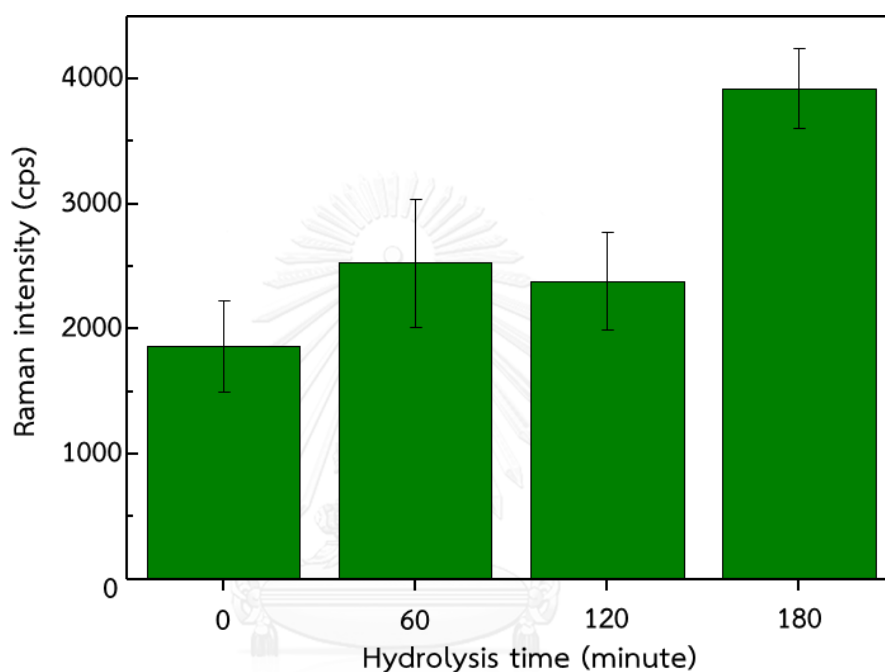


Figure 4.11 The relationship between Raman intensity at  $1201\text{ cm}^{-1}$  and hydrolysis time.

#### 4.6. Effect of 4-ATP concentration in diazotization reaction

In order to improve a selective and sensitive procedure for carbofuran detection, the effect of the 4-ATP concentration has to be studied. The 4-ATP is a main substance in diazotization (Figure 4.12), which has been recently used as a probe molecule to estimate enhancement activity of SERS substrate. It can bind easily on the metal surface *via* metal-S bond [48, 53].

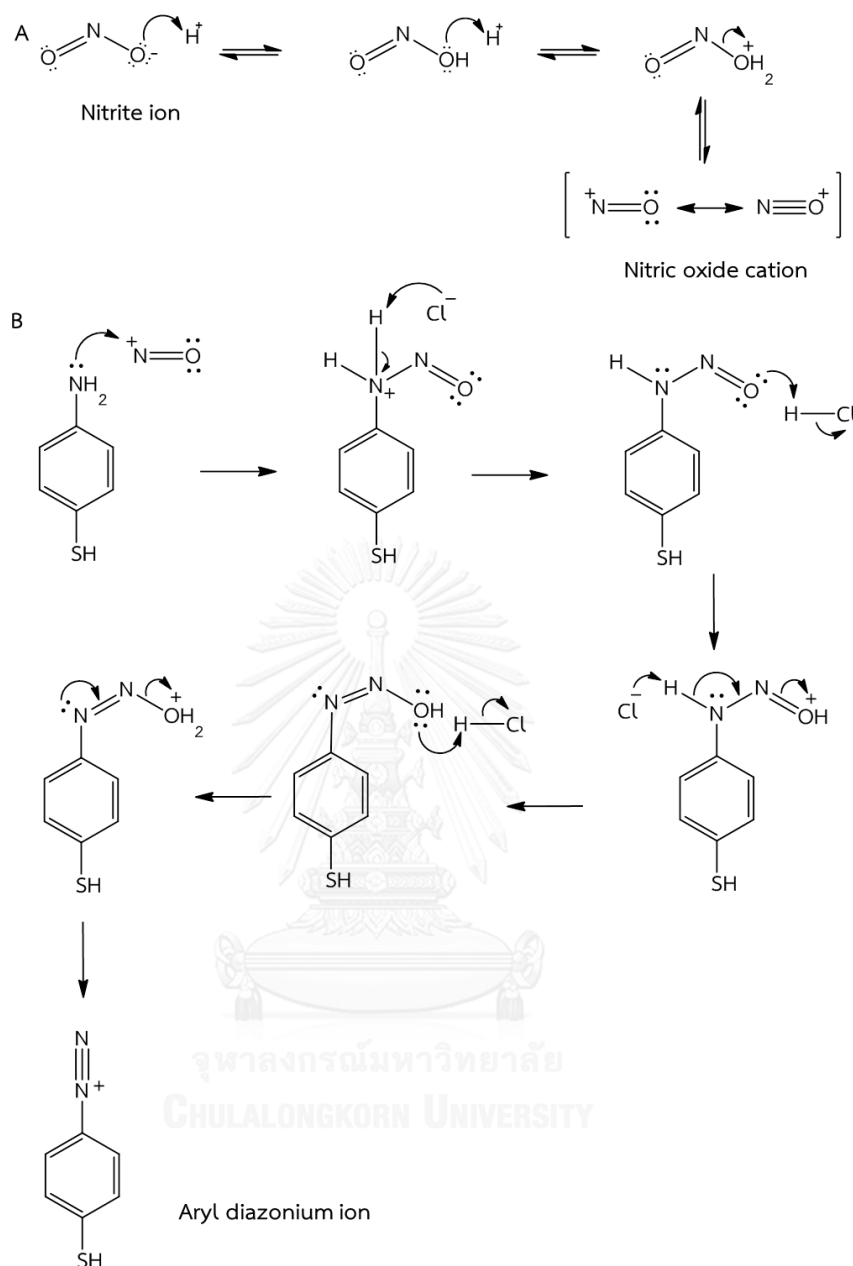


Figure 4.12 Mechanism of diazotization for the formation of diazonium ion.

In this study, we use the 4-ATP as a linked molecule between carbofuran phenol and the surface of AgNPs to promote the effective adsorption for SERS measurement. On one side of the 4-ATP molecule, an amino group ( $-\text{NH}_2$ ) is functionalized by  $\text{NaNO}_2$  under acidic condition to create aryl diazonium ion ( $\text{Ph}-\text{N}^+\equiv\text{N}$ ), which specifically reacts with phenolic compounds (carbofuran phenol in

this work) to give an azo compound. On the other side of the 4-ATP molecule, a thiol group (-SH) is connected effectively with the surface of metal nanoparticles.

To obtain the optimal amount of 4-ATP in this protocol giving highest SERS intensity, various concentrations of 4-ATP (0.5–3 mM) in acidic solution were carefully examined. SERS spectra of the azo compound, which is generated from different 4-ATP concentrations, are shown in Figure 4.13. In diazo coupling reaction, a  $-N^+\equiv N$  group of aryl diazonium salt reacts with carbofuran phenol to generate C-N with carbon atom of phenol ring that cause peaks at 1410, 1379, 1333 and 1201  $\text{cm}^{-1}$ , which are assigned in Table 4.1. As the SERS spectra of azo compound created from 0.5 and 3 mM, their Raman intensity are unnoticeable. For 0.5 mM, the amount of diazonium ion is not enough to react totally with that of target analyte in a minute while, for 3 mM, the quantity of acid is insufficient to stabilize diazonium ions to be ready in coupling reaction. As the most noticeable peak position of azo compound in Figure 4.8, Raman intensity at 1201  $\text{cm}^{-1}$ , which attributes to CN stretching, CH and OH bending, CNN in plane bending and CC stretching, of azo compound from 1 mM 4-ATP solution attains the highest intensity. The amount of 4-ATP molecule at 1 mM is also in the good proportion with that of  $\text{NaNO}_2$  and HCl to form  $-N^+\equiv N$  ion for a coupling reaction. Hence, the optimized concentration of 4-ATP for this protocol is at 1 mM 4-ATP.



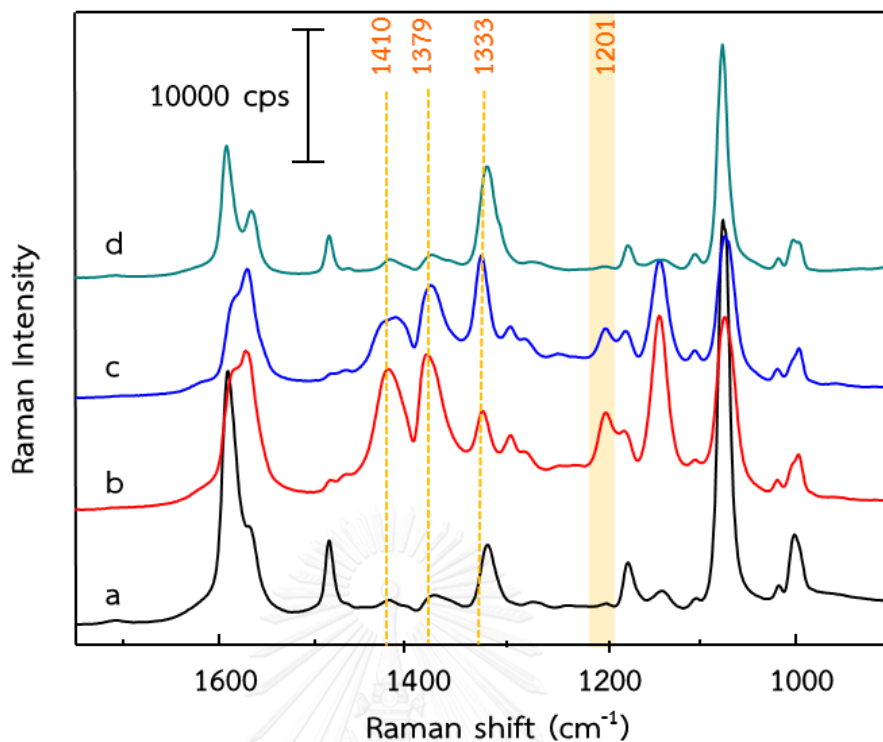


Figure 4.13 SERS spectra of the azo compound generated using 100 ppm carbofuran phenol with various concentrations of 4-ATP: (a) 0.5, (b) 1, (c) 2 and (d) 3 mM, respectively (The incubation time of diazotization is 1 minute).

#### 4.7 Effect of incubation time in coupling reaction

To obtain the complete chemical reaction between diazonium ion and carbofuran phenol, the incubation time was carefully considered as an essential factor in a facile and brief carbofuran detection method. The overall mechanism of diazo coupling reaction between carbofuran phenol and diazonium ion generated from 4-ATP was illustrated in Figure 4.14. To test the suitable time, the combination between carbofuran phenol and diazonium ion was incubated in iced-water bath for 1–180 minutes. Figure 4.15 shows the correlation of Raman intensity at  $1201\text{ cm}^{-1}$ , which is obviously an evident characteristic band of azo compound, with the incubation time in coupling reaction. The standard deviations of each sample are 1287.54, 1422.34, 582.43, 859.74, and 2147.17 for 1, 30, 60, 120, and 180 minutes, respectively. Raman intensity reasonably increases with an increase in incubation

time. In the range of 1–120 minutes, their Raman intensities are insignificantly different. SERS spectrum of three hour-solution is obtained with the highest intensity and variation. As an empirical method, the incubation time at a minute is selected for a diazo coupling reaction. The diazonium ions completely react to carbofuran phenol with an acceptable time.

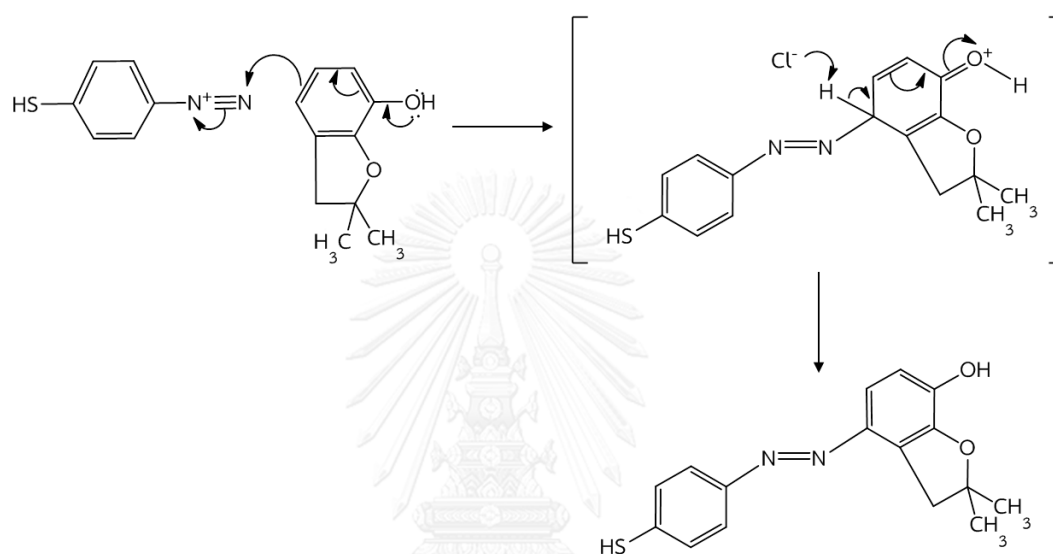


Figure 4. 14 Mechanism of diazo coupling reaction between carbofuran phenol and diazonium ion generated from 4-ATP.

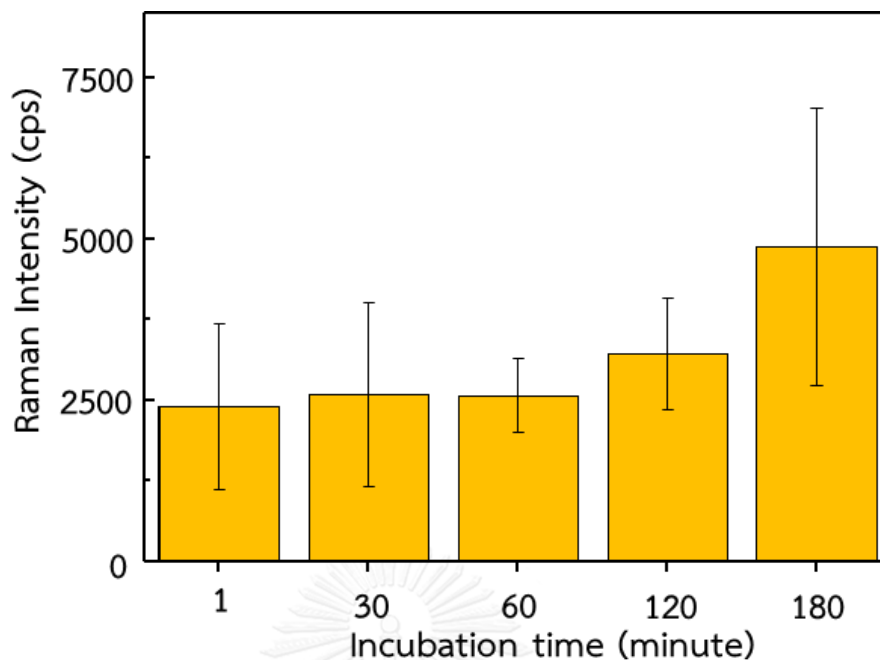


Figure 4.15 The correlation of Raman intensity at  $1201\text{ cm}^{-1}$  with the incubation time.

#### 4.8 Diazo-coupling-based SERS for carbofuran detection

After studying the optimal condition for the effective method of carbofuran analysis, various concentrations of carbofuran were determined to investigate the potential of our developed protocol. To examine the efficiency of this proposed method, the various concentrations of carbofuran phenol from 0–1000 ppm in alkaline solution were added into the diazonium solution for a coupling reaction. Before collecting SERS spectra, the solution of azo compound was mixed together with silver colloid.

From Figure 4.16, the Raman intensity of azo compound decreases with a decrease in carbofuran concentration. However, signals of SERS spectrum can still be observed at 0 ppm carbofuran. It is a spectrum of molecules decomposed from diazonium ions, as discussed previously. To analyze the concentrations of carbofuran, the ratio of Raman intensity at  $1201\text{ cm}^{-1} / 1021\text{ cm}^{-1}$  and  $1201\text{ cm}^{-1} / 1075\text{ cm}^{-1}$  were plots against the concentrations of carbofuran as shown in Figure 4.17 (A1, B1). According to the peak assignments of azo compound (Table 4.1), the

peak at  $1021\text{ cm}^{-1}$  refers to aromatic =C-H in plane deformation vibration of phenyl ring and the peak at  $1075\text{ cm}^{-1}$  represents to C-S stretching of molecules connected on AgNPs surface. To use these two peak ratios for determining the amount of carbofuran, Figure 4.17 (A2, B2) illustrate the linearity of Raman intensity ratios against the concentration of carbofuran in the range of 0.1–5 ppm. It was found that the linearity of  $R^2 = 0.9891$  and  $R^2 = 0.9666$  were observe from using ratio of  $1201\text{ cm}^{-1} / 1021\text{ cm}^{-1}$  and  $1201\text{ cm}^{-1} / 1075\text{ cm}^{-1}$ , respectively. According to obtained  $R^2$ , the ratio of  $1201\text{ cm}^{-1} / 1021\text{ cm}^{-1}$  is chosen as the effective responses to quantify amount of carbofuran. The linear equation is shown as  $y = 0.0898x + 0.0410$ , where y is the intensity ratio and x is the concentration of carbofuran (ppm). The detection limit of proposed protocol is 0.729 ppm. Even our developed method cannot overcome mainstream conventional methods such as LC-MS, GC-MS and biosensors with the detection limit ranging from 0.01 to 0.10 ppm [3, 7, 8, 56, 57], it is still comparable. Moreover, the combination of diazo coupling reaction and SERS provides a rapid and selective detection method with no requirement of separation or chromatographic processes as in LC-MS and GC-MS.



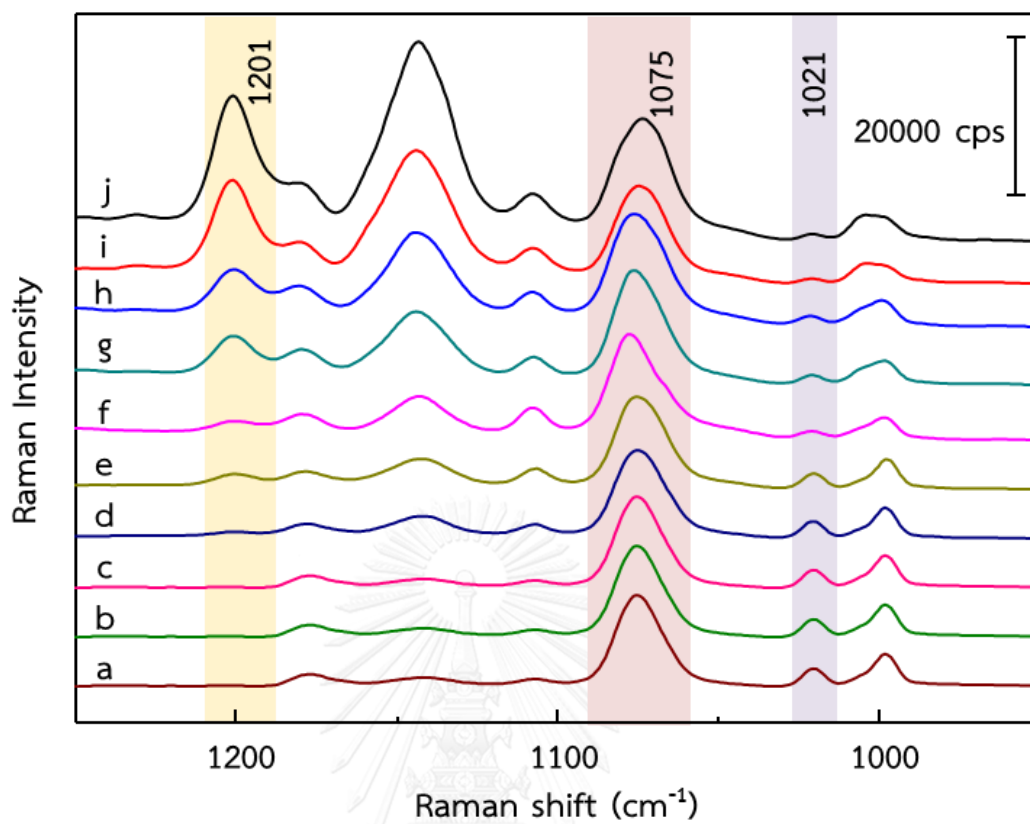


Figure 4.16 SERS spectra of azo compound generated from (a) 0, (b) 0.1, (c) 0.5, (d) 1, (e) 5, (f) 10, (g) 50, (h) 100, (i) 500 and (j) 1000 ppm carbofuran.

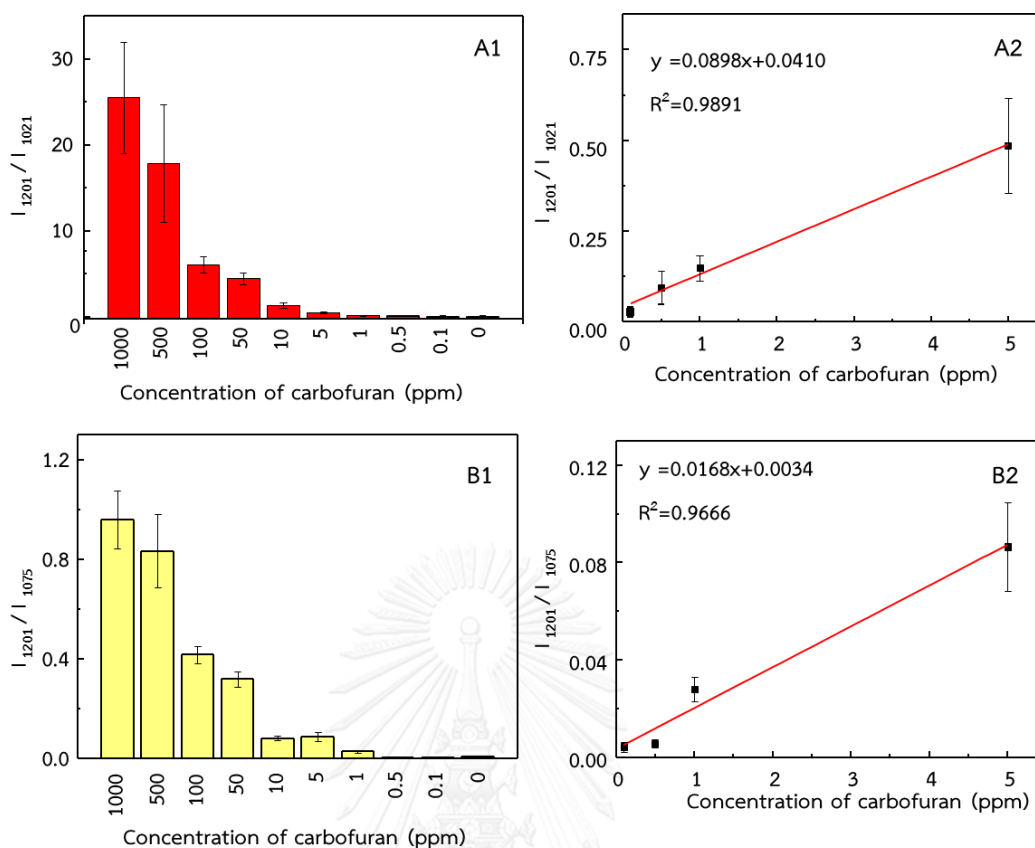


Figure 4.17 The intensity ratios of  $1201\text{ cm}^{-1} / 1021\text{ cm}^{-1}$  (A1) and  $1201\text{ cm}^{-1} / 1075\text{ cm}^{-1}$  (B1) versus the concentration of carbofuran and the relation between the intensity ratios of  $1201\text{ cm}^{-1} / 1021\text{ cm}^{-1}$  (A2) and  $1201\text{ cm}^{-1} / 1075\text{ cm}^{-1}$  (B2) versus the concentration of carbofuran in the range of 0.1-5 ppm.

#### 4.9 Effect of interfering substances on the detection method

According to the objectives of this research, we have designed and developed the method to detect the amount of carbofuran residue. For practical applications, the influence of interfering substances is carefully considered. In this part, we studied the effect of nine interfering substances, namely acetic acid, ascorbic acid, formic acid, fructose, glucose, lactose, maltose, NaCl, and table sugar on the effectiveness of proposed carbofuran detection. We chose these substances because they are naturally found in fruits and vegetables. Thus, the study of their effect in our system is firmly required.

Figure 4.18 illustrates the intensity ratio from azo compound generated from 5 ppm carbofuran in the solution with various types of interfering substances. Without interfering substance, the intensity ratio is around 0.49 with a standard deviation of 0.13. For sample interfered with acid, the intensity ratios are 0.66, 0.61, and 0.67 for acetic acid, ascorbic acid and formic acid, respectively. They are slightly higher than that of other samples because a  $-N^+\equiv N$  group of aryl diazonium salt is more stable in acidic solution, which promotes the azo coupling reaction. For other interfering substances, the calculated intensity ratios are 0.44, 0.48, 0.38, 0.51, 0.57, and 0.50 for fructose, glucose, lactose, maltose, NaCl and table sugar, respectively. They are in the variation of no interference. Therefore, the carbofuran analysis from our protocol is not significantly influenced by the studied interfering substances.

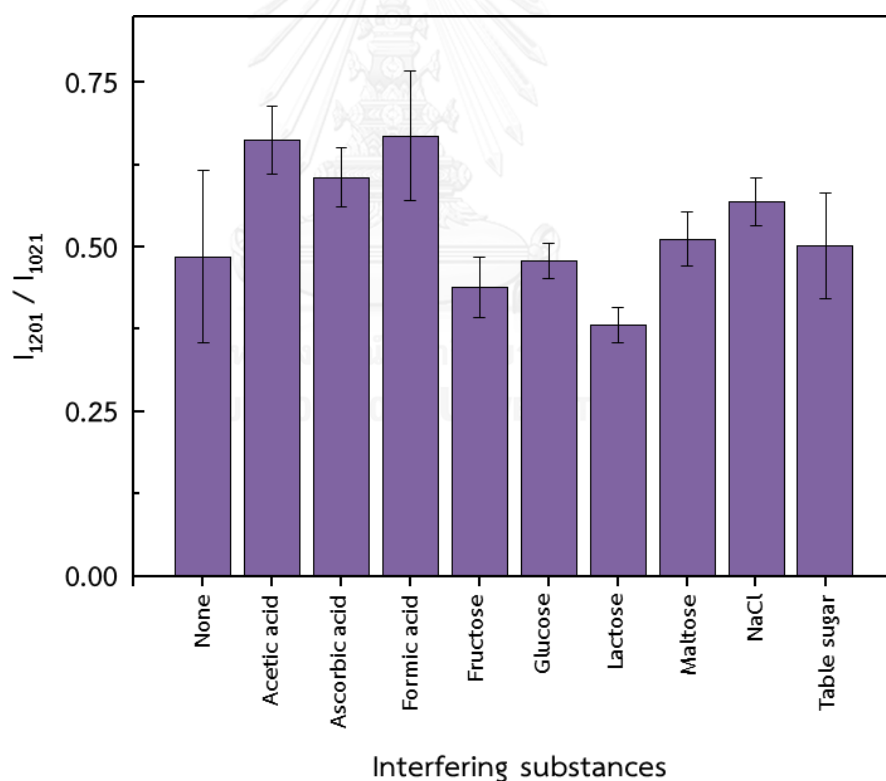


Figure 4.18 The intensity ratios between peaks at 1201 and 1021  $\text{cm}^{-1}$  from SERS spectra of azo compound generated from 5 ppm carbofuran in the presence of 1mM interfering substance.

#### 4.10 Carbofuran analysis in real samples using our developed method

For practical analysis, the effectiveness of carbofuran detection in agricultural products is investigated. We chose the samples such as rice, soya bean, white pepper, black pepper, mung bean, sesame, peanut and chili pepper because they are the common agricultural products in the market, which are usually contaminated by high level of carbofuran residues. Then, carbofuran was spiked into the real samples in order to simulate the contaminated real samples.

To quantify the amount of carbofuran spiked on each sample, the Raman intensity ratio between peaks at 1201 and 1021  $\text{cm}^{-1}$  were linearly plotted against the concentration of carbofuran in the range of 0.1–5 ppm, as shown in Figure 4.19. In this range, they illustrate the linear graph with  $R^2 = 0.91\text{--}0.97$ . From the linear equation for each sample,  $y$  is the intensity ratio and  $x$  is the concentration of carbofuran (ppm). The limits of detections of this protocol are 2.043, 0.245, 0.406, 1.190, 1.144, 1.364, 3.391, and 0.429 ppm for rice, soya bean, white pepper, black pepper, mung bean, sesame, peanut, and chili pepper, respectively. By comparison with the detection limit of standard solution (0.605 ppm), the more effective limit of detection can be occurred in soya bean, white pepper and chili pepper. To restrict the level of carbofuran residues in Thai agricultural products, the maximum residue limits (MRLs) of Thai agricultural standard are established as illustrated in Table 4.2 [58]. In this experiment, 5 mL of ethanol was used to extract carbofuran residues in 5 grams of each sample. Thus, in this case, the units of detection limit between ppm (mg/L) and mg/kg are comparable. The limits of detection are approximately equal to the MRLs of each sample on except for rice and peanut. Since, they are closely comparable as a rapid and selective method without purification or separation process.



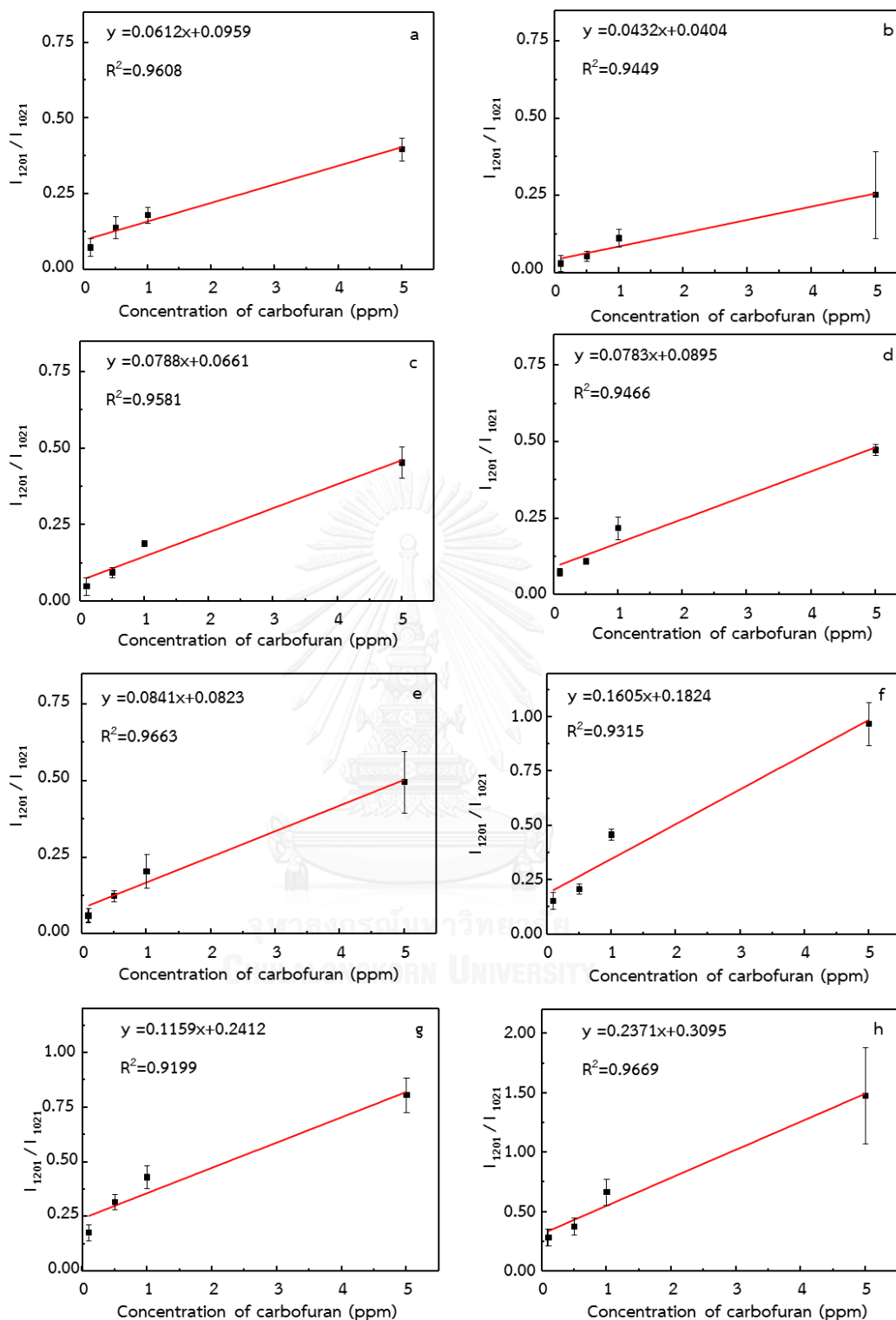


Figure 4.19 The relation between the intensity ratios and concentration of carbofuran in the range of 0.1–5 ppm from agricultural products, *i.e.*, (a) rice, (b) soya bean, (c) white pepper, (d) black pepper, (e) mung bean, (f) sesame, (g) peanut, and (h) chili pepper.

Table 4.2 Maximum residue limits (MRLs) of each agricultural product.

Commodities	Maximum Residue Limits (MRLs) (mg/kg)
Rice	0.1
Soya bean	0.2
White pepper	1
Black pepper	1
Mung bean	0.2
Sesame	0.1
Peanut	0.1
Chili pepper	5

According to the detection limit of the purposed method (0.729 ppm), the recovery percentage of 1 ppm and 5 ppm carbofuran introduced on the studied samples was investigated to estimate the accuracy in carbofuran detection. Figure 4.20 shows the recovery percentage of 1 and 5 ppm carbofuran, which is spiked on the agricultural products. To rinse away 5 ppm carbofuran from sesame, peanut and chili pepper, the recovery percentages are higher than 200% but they are approximately 100 % for another five samples. For 1 ppm carbofuran, the recovery percentages are lower than 200 % except sesame, peanut and chili pepper. The recovery percentage of 1 ppm is larger than that of 5 ppm because there are some interfering substances, which can strongly affect the carbofuran detection at lower concentration. The slight differences on the recovery percentage of the both systems were observed from rice, soya bean, white pepper, black pepper and mung bean, while the large variations of the recovery percentage were found on sesame, peanut and chili pepper. Furthermore, it can be seen that the recovery percentage of the carbofuran on especially sesame, peanut and chili pepper are higher than the amount of cabofuran added in the system. This suggests that there are some derivatives of phenol which might be leaching during the detection process. These leaking compounds are possibly reacted with the diazonium ions to form the azo

compounds. This phenomenon will disturb the detection as the amount of carbofuran was determined from the generated azo compounds. The observed Raman intensity ratio of peak at  $1201$  and  $1021\text{ cm}^{-1}$  can be enhanced according to the interferences. As far as we known, the main phenol derivatives found in the sesame, peanut and chili pepper are tocopherol, catechol and capsaicin *etc.*, respectively [59-63]. From this observation, the effectiveness of this carbofuran analysis can be strongly influenced by the types of the agricultural products containing natural phenolic compounds.

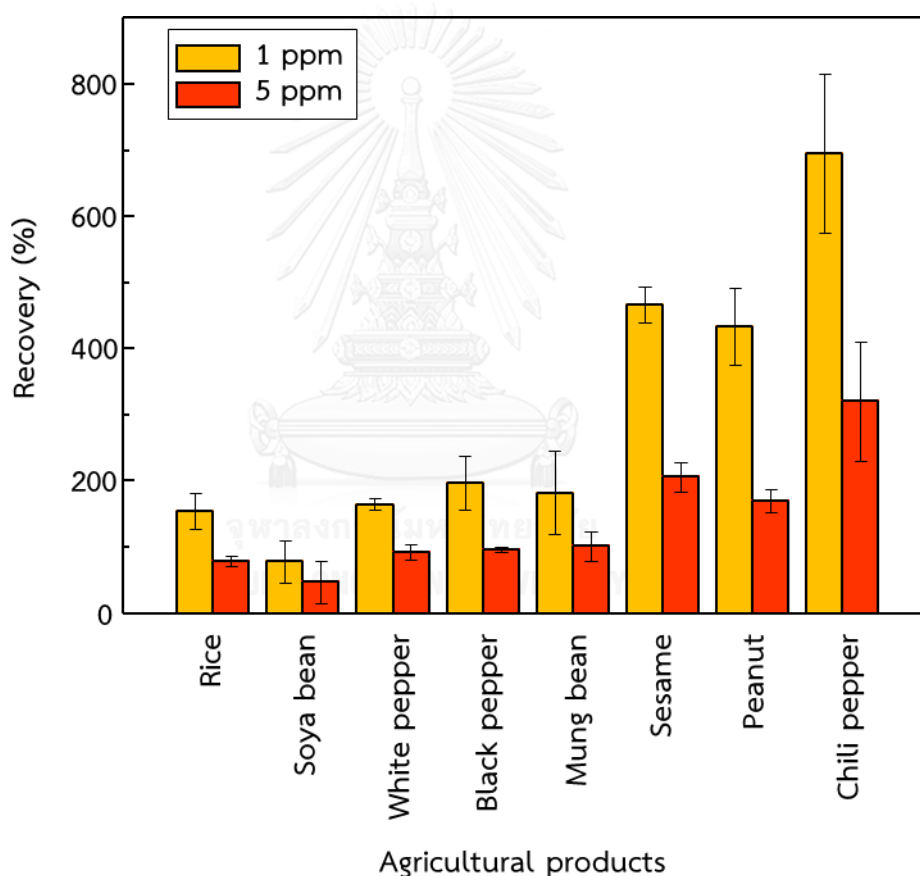


Figure 4.20 The recovery percentage of 0.1 and 5 ppm carbofuran, which is spiked on the samples.

## CHAPTER 5

### CONCLUSIONS

According to our designed and developed protocol, we have combined the diazo coupling reaction and AgNPs as a SERS substrate for selective and sensitive analysis of carbofuran. With low affinity of carbofuran on AgNPs surface, carbofuran is required to be hydrolyzed into carbofuran phenol in order to use in the diazo coupling reaction. The coupling reaction is underwent the corresponding carbofuran phenol. This step is extremely significant for creating the azo compound containing a thiol group. The highly strong SERS signal can be achieved according to the deposition of the generated azo compound on the surface of AgNPs *via* Ag-S bond. To directly quantify amount of carbofuran from carbofuran phenol, the optimal conditions are the hydrolysis time at 3 hours, 1 mM of 4-ATP acidic solution and the incubation time of diazo-coupling at 1 minute. To investigate the efficiency of this proposed method, the Raman intensity ratios of peaks at 1201 and 1021  $\text{cm}^{-1}$  from SERS spectra of azo compound were plotted against the concentrations of carbofuran. These two peaks mainly refer to the C-N stretching and aromatic =C-H in plane deformation as the characteristic bands of azo compound and phenyl ring on AgNPs surface, respectively. In this case, the peak at 1021  $\text{cm}^{-1}$  was chosen as a background signal because it does not associate with the formation of azo compound. From the observation, the linear calibration curve of Raman intensity ratio with  $R^2 = 0.9891$  was achieved in the range of carbofuran concentrations from 5 to 0.1 ppm and the limit of detection (LOD) is 0.729 ppm. Moreover, the efficiency of carbofuran determination using our proposed method was not significantly influenced by the interfering substances such as acetic acid, ascorbic acid, formic acid, fructose, glucose, lactose, maltose, NaCl, and table sugar. For practical application, this developed protocol was also considered to monitor the amount of artificial added carbofuran in agricultural products, for instance rice, soya bean, white pepper, black pepper, mung bean, sesame, peanut and chili pepper. Within the range of carbofuran concentration from 0.1 to 5 ppm, the calculated linear

calibration curves with  $R^2 = 0.91\text{--}0.97$  were occurred. The detection limits were in the range of 0.5–3 ppm. To control the high level of carbofuran residues in the market, our proposed protocol in this research is promising as it is a rapid, selective and practical detection method without any complicated separation.



## REFERENCES

1. Duangchinda, A., Anurugsa, B. and Hungspreug, N., The use of organophosphate and carbamate Pesticides on paddy fields and cholinesterase levels of farmers in Sam chuk district, Suphan buri province, Thailand. *Thammasat International Journal of Science and Technology*, **2014. 19**: p. 39-51.
2. *Guidelines for Canadian drinking water quality*. 1991, Health and Welfare Canada: Ottawa, Ontario.
3. Skládal, P., Nunes, G.S., Yamanaka, H. and Ribeiro, M.L., Detection of carbamate pesticides in vegetable samples using cholinesterase-based biosensors. *Electroanalysis*, **1997. 9**: p. 1083-1087.
4. Delfino, R.T., Ribeiro, T.S. and Figueroa-Villar, J.D., Organophosphorus compounds as chemical warfare agents: a review. *Journal of the Brazilian Chemical Society*, **2009. 20**: p. 407-428.
5. Cambon, C., Declume, C. and Derache, R., Effect of the insecticidal carbamate derivatives (carbofuran, pirimicarb, aldicarb) on the activity of acetylcholinesterase in tissues from pregnant rats and fetuses. *Toxicology and Applied Pharmacology*, **1979. 49**: p. 203-208.
6. Dutra, B.K., Fernandes, F.A., Lauffer, A.L. and Oliveira, G.T., Carbofuran-induced alterations in the energy metabolism and reproductive behaviors of *Hyaella castroi* (Crustacea, Amphipoda). *Comparative Biochemistry and Physiology Part C: Toxicology & Pharmacology*, **2009. 149**: p. 640-646.
7. Li, X., Gan, P., Peng, R., Huang, C. and Yu, H., Determination of 23 Organophosphorous Pesticides in Surface Water Using SPME Followed by GC-MS. *Journal of Chromatographic Science*, **2010. 48**: p. 183-187.
8. Nelsen, T.R., Cook, R.F., Gruenauer, M.H., Gilbert, M.D. and Witkonton, S., Determination of the phenolic metabolites of carbofuran in plants by gas

- chromatography/mass spectrometry. *Journal of Agricultural and Food Chemistry*, **1983**. **31**: p. 1147-1150.
9. Zhu, P., Miao, H., Du, J., Zou, J., Zhang, G., Zhao, Y.F. and Wu, Y.N., Organochlorine Pesticides and Pyrethroids in Chinese Tea by Screening and Confirmatory Detection Using GC-NCI-MS and GC-MS/MS. *Journal of Agricultural and Food Chemistry*, **2014**. **62**: p. 7092-7100.
  10. Sánchez-Cortés, S., Domingo, C., García-Ramos, J.V. and Aznárez, J.A., Surface-Enhanced Vibrational Study (SEIR and SERS) of Dithiocarbamate Pesticides on Gold Films. *Langmuir*, **2001**. **17**: p. 1157-1162.
  11. Zhang, L., Self-assembly Ag nanoparticle monolayer film as SERS Substrate for pesticide detection. *Applied Surface Science*, **2013**. **270**: p. 292-294.
  12. Vongsivut, J., Robertson, E.G. and McNaughton, D., Surface-enhanced Raman spectroscopic analysis of fonofos pesticide adsorbed on silver and gold nanoparticles. *Journal of Raman Spectroscopy*, **2010**. **41**: p. 1137-1148.
  13. Tang, H., Fang, D., Li, Q., Cao, P., Geng, J., Sui, T., Wang, X., Iqbal, J. and Du, Y., Determination of Tricyclazole Content in Paddy Rice by Surface Enhanced Raman Spectroscopy. *Journal of Food Science*, **2012**. **77**: p. T105-T109.
  14. Fan, Y., Lai, K., Rasco, B.A. and Huang, Y., Analyses of phosmet residues in apples with surface-enhanced Raman spectroscopy. *Food Control*, **2014**. **37**: p. 153-157.
  15. Eric, C.L.R. and Pablo, G.E., *Principles of surface enhanced Raman spectroscopy and related plasmonic effects*. first edition ed. 2009, Radarweg 29, PO Box 211, 1000 AE Amsterdam, The Netherlands Linacre House, Jordan Hill, Oxford OX2 8DP, UK: Elsevier.
  16. Abalde-Cela, S., Aldeanueva-Potel, P., Mateo-Mateo, C., Rodríguez-Lorenzo, L., Alvarez-Puebla, R.A. and Liz-Marzán, L.M., Surface-enhanced Raman scattering biomedical applications of plasmonic colloidal particles. *Journal of The Royal Society Interface*, **2010**. **7**: p. S435-S450.
  17. Gabudean, A.M., Biro, D. and Astilean, S., Localized surface plasmon resonance (LSPR) and surface-enhanced Raman scattering (SERS) studies of 4-

- aminothiophenol adsorption on gold nanorods. *Journal of Molecular Structure*, **2011. 993**: p. 420-424.
18. Chen, Y. and Ming, H., Review of surface plasmon resonance and localized surface plasmon resonance sensor. *Photonic Sensors*, **2012. 2**: p. 37-49.
  19. Willets, K.A. and Duyne, R.P.V., Localized Surface Plasmon Resonance Spectroscopy and Sensing. *Annual Review of Physical Chemistry*, **2007. 58**: p. 267-297.
  20. Geddes, C.D., Aslan, K., Gryczynski, I., Malicka, J. and Lakowicz, J.R., *Noble-Metal Surfaces for Metal-Enhanced Fluorescence*, in *Reviews in Fluorescence 2004*, C.D. Geddes and J.R. Lakowicz, Editors. 2004, Springer US: Boston, MA. p. 365-401.
  21. Goulet, P.J.G. and Aroca, R.F., *Surface-Enhancement of Fluorescence Near Noble Metal Nanostructures*, in *Radiative Decay Engineering*, C.D. Geddes and J.R. Lakowicz, Editors. 2005, Springer US: Boston, MA. p. 223-247.
  22. Zeng, J., Liang, D. and Cao, Z. *Applications of optical fiber SPR sensor for measuring of temperature and concentration of liquids*. 2005.
  23. Petryayeva, E. and Krull, U.J., Localized surface plasmon resonance: Nanostructures, bioassays and biosensing—A review. *Analytica Chimica Acta*, **2011. 706**: p. 8-24.
  24. Neubrech, F., Dregely, D., Zhao, J. and Giessen, H. *Nanoantenna-enhanced mid-IR vibration spectroscopy with single molecular layer sensitivity*. in *2013 38th International Conference on Infrared, Millimeter, and Terahertz Waves (IRMMW-THz)*. 2013.
  25. Abb, M., Wang, Y., Papisimakis, N., de Groot, C.H. and Muskens, O.L., Surface-Enhanced Infrared Spectroscopy Using Metal Oxide Plasmonic Antenna Arrays. *Nano Letters*, **2014. 14**: p. 346-352.
  26. Rodríguez-Lorenzo, L., Álvarez-Puebla, R.A., de Abajo, F.J.G. and Liz-Marzán, L.M., Surface Enhanced Raman Scattering Using Star-Shaped Gold Colloidal Nanoparticles. *The Journal of Physical Chemistry C*, **2010. 114**: p. 7336-7340.



27. Mora, A., Comejo, J., Revilla, E. and Hermosin, M.C., Persistence and degradation of carbofuran in Spanish soil suspensions. *Chemosphere*, **1996**. **32**: p. 1585-1598.
28. Kuo, W.S., Chiang, Y.H. and Lai, L.S., Degradation of Carbofuran in Water by Solar Photocatalysis in Presence of Photosensitizers. *Journal of Environmental Science and Health, Part B*, **2006**. **41**: p. 937-948.
29. Wei, H., Sun, J.J., Wang, Y.M., Li, X. and Chen, G.N., Rapid hydrolysis and electrochemical detection of trace carbofuran at a disposable heated screen-printed carbon electrode. *Analyst*, **2008**. **133**: p. 1619-1624.
30. Chen, L., Jia, C., Zhao, E., He, M., Yu, P. and Zhu, X., Gas Chromatography–Mass Spectroscopy Analysis of Carbofuran and Its Metabolite 3-Hydroxycarbofuran in Maize and Soil in Field. *Communications in Soil Science and Plant Analysis*, **2011**. **42**: p. 1316-1323.
31. de Melo Plese, L.P., Paraiba, L.C., Foloni, L.L. and Pimentel Trevizan, L.R., Kinetics of carbosulfan hydrolysis to carbofuran and the subsequent degradation of this last compound in irrigated rice fields. *Chemosphere*, **2005**. **60**: p. 149-156.
32. Yu, C.-C., Booth, G.M., Hansen, D.J. and Larsen, J.R., Fate of carbofuran in a model ecosystem. *Journal of Agricultural and Food Chemistry*, **1974**. **22**: p. 431-434.
33. Seiber, J.N., Catahan, M.P. and Barril, C.R., Loss of carbofuran from rice paddy water: Chemical and physical factors. *Journal of Environmental Science and Health, Part B*, **1978**. **13**: p. 131-148.
34. Brahmaprakash, G.P., Panda, S. and Sethunathan, N., Relative persistence of hexachlorocyclohexane, methyl parathion and carbofuran in an alluvial soil under flooded and non-flooded conditions. *Agriculture, Ecosystems & Environment*, **1987**. **19**: p. 29-39.
35. Talebi, K. and Walker, C.H., A comparative study of carbofuran metabolism in treated and untreated soils. *Pesticide Science*, **1993**. **39**: p. 65-69.
36. Chiron, S., Torres, J.A., Fernandez-alba, A., Alpendurada, M.F. and Barcelo, D., Identification of Carbofuran And Methiocarb and their Transformation

- Products in Estuarine Waters by On-line Solid Phase Extraction Liquid Chromatography—Mass Spectrometry. *International Journal of Environmental Analytical Chemistry*, **1996**. **65**: p. 37-52.
37. Bailey, H.C., Digiorio, C., Kroll, K., Hinton, D.E., Miller, J.L. and Starrett, G., Development of procedures for identifying pesticide toxicity in ambient waters: Carbofuran, diazinon, chlorpyrifos. *Environmental Toxicology and Chemistry*, **1996**. **15**: p. 837-845.
38. Mustroph, H., Studies on the UV-vis absorption spectra of azo dyes: Part 25. 11For Part 24 see Mustroph, H. & Gussmann, F., *J. Prakt. Chem.*, 332 (1990) 93. analysis of the fine structure of the  $\pi\pi^* \rightarrow \pi\pi^*$  band of 4<sup>l</sup>-donor-sub. *Dyes and Pigments*, **1991**. **15**: p. 129-137.
39. Shah, T.B., Shiny, R.S., Dixit, R.B. and Dixit, B.C., Synthesis and dyeing properties of new disazo disperse dyes for polyester and nylon fabrics. *Journal of Saudi Chemical Society*, **2014**. **18**: p. 985-992.
40. Gulcan, M., Karataş, Y., Işık, S., Öztürk, G., Akbaş, E. and Şahin, E., Transition Metal(II) Complexes of a Novel Symmetrical Benzothiazole-Based Ligand: Synthesis, Spectral/Structural Characterization and Fluorescence Properties. *Journal of Fluorescence*, **2014**. **24**: p. 1679-1686.
41. Han, X.X., Pienpinijtham, P., Zhao, B. and Ozaki, Y., Coupling Reaction-Based Ultrasensitive Detection of Phenolic Estrogens Using Surface-Enhanced Resonance Raman Scattering. *Analytical Chemistry*, **2011**. **83**: p. 8582-8588.
42. Lee, P.C. and Meisel, D., Adsorption and surface-enhanced Raman of dyes on silver and gold sols. *The Journal of Physical Chemistry*, **1982**. **86**: p. 3391-3395.
43. Mammone, J.F., Sharma, S.K. and Nicol, M., Raman spectra of methanol and ethanol at pressures up to 100 kbar. *The Journal of Physical Chemistry*, **1980**. **84**: p. 3130-3134.
44. Yu, Y., Lin, K., Zhou, X., Wang, H., Liu, S. and Ma, X., New C–H Stretching Vibrational Spectral Features in the Raman Spectra of Gaseous and Liquid Ethanol. *The Journal of Physical Chemistry C*, **2007**. **111**: p. 8971-8978.

45. Krutyakov, Y.A., Kudrinskiy, A.A., Olenin, A.Y. and Lisichkin, G.V., Synthesis and properties of silver nanoparticles: advances and prospects. *Russian Chemical Reviews*, **2008**. **77**: p. 233-257.
46. Wagener, P., Schwenke, A. and Barcikowski, S., How Citrate Ligands Affect Nanoparticle Adsorption to Microparticle Supports. *Langmuir*, **2012**. **28**: p. 6132-6140.
47. Gutierrez, L., Aubry, C., Cornejo, M. and Croue, J.P., Citrate-Coated Silver Nanoparticles Interactions with Effluent Organic Matter: Influence of Capping Agent and Solution Conditions. *Langmuir*, **2015**. **31**: p. 8865-8872.
48. Zheng, J., Zhou, Y., Li, X., Ji, Y., Lu, T. and Gu, R., Surface-Enhanced Raman Scattering of 4-Aminothiophenol in Assemblies of Nanosized Particles and the Macroscopic Surface of Silver. *Langmuir*, **2003**. **19**: p. 632-636.
49. Briegleb, G., *Elektron Donator-Acceptor Komplex*. 1961, Berlin: Springer-Verlag.
50. Parnklang, T., Lertvachirapaiboon, C., Pienpinijtham, P., Wongravee, K., Thammacharoen, C. and Ekgasit, S., H<sub>2</sub>O<sub>2</sub>-triggered shape transformation of silver nanospheres to nanoprisms with controllable longitudinal LSPR wavelengths. *RSC Advances*, **2013**. **3**: p. 12886-12894.
51. Link, S. and El-Sayed, M.A., Shape and size dependence of radiative, non-radiative and photothermal properties of gold nanocrystals. *International Reviews in Physical Chemistry*, **2000**. **19**: p. 409-453.
52. Persson, B.N.J., Polarizability of small spherical metal particles: influence of the matrix environment. *Surface Science*, **1993**. **281**: p. 153-162.
53. Xu, B., Gonella, G., DeLacy, B.G. and Dai, H.L., Adsorption of Anionic Thiols on Silver Nanoparticles. *The Journal of Physical Chemistry C*, **2015**. **119**: p. 5454-5461.
54. Socrates, G., *Infrared and Raman characteristic group frequencies : tables and charts*. third ed. 2001, England: John Wiley & Sons Ltd.
55. Yan, Q.X., Hong, Q., Han, P., Dong, X.J., Shen, Y.J. and Li, S.P., Isolation and characterization of a carbofuran-degrading strain *Novosphingobium* sp. FND-3. *FEMS Microbiology Letters*, **2007**. **271**: p. 207-213.

56. Zomer, E., Saul, S. and Charm, S.E., *Test kit for determination of organophosphate and carbamate pesticides with insect's brain material that hydrolyses a 6-substituted D luciferin ester*. 1994: U.S.
57. Sun, X., Du, S., Wang, X., Zhao, W. and Li, Q., A Label-Free Electrochemical Immunosensor for Carbofuran Detection Based on a Sol-Gel Entrapped Antibody. *Sensors (Basel, Switzerland)*, **2011**. **11**: p. 9520-9531.
58. *The Thai Agricultural Standards on Pesticide Residues: Maximum Residue Limits*. 2008, National Bureau of Agricultural Commodity and Food Standards The Royal Gazette Vol. 125 Special Section 139D.
59. Rangkadilok, N., Pholphana, N., Mahidol, C., Wongyai, W., Saengsooksree, K., Nookabkaew, S. and Satayavivad, J., Variation of sesamin, sesamol and tocopherols in sesame (*Sesamum indicum* L.) seeds and oil products in Thailand. *Food Chemistry*, **2010**. **122**: p. 724-730.
60. Cooney, R.V., Custer, L.J., Okinaka, L. and Franke, A.A., Effects of Dietary Sesame Seeds on Plasma Tocopherol Levels. *Nutrition and Cancer*, **2001**. **39**: p. 66-71.
61. Stansbury, M.F. and Hoffpauir, C.L., Estimation of skin content of peanut meals and relative skin pigment content of isolated proteins. *Journal of the American Oil Chemist' Society*, **1952**. **29**: p. 370-372.
62. Swain, J. and Kumar Mishra, A., Location, Partitioning Behavior, and Interaction of Capsaicin with Lipid Bilayer Membrane: Study Using Its Intrinsic Fluorescence. *The Journal of Physical Chemistry B*, **2015**. **119**: p. 12086-12093.
63. Janssens, P.L.H.R., Hursel, R., Martens, E.A.P. and Westerterp-Plantenga, M.S., Acute Effects of Capsaicin on Energy Expenditure and Fat Oxidation in Negative Energy Balance. *PLoS ONE*, **2013**. **8**: p. e67786.







จุฬาลงกรณ์มหาวิทยาลัย  
CHULALONGKORN UNIVERSITY









**VITA**

Name: Miss Thanyada Sukmanee  
Date of Birth: 17 July 1990 Birth place: Phitsanulok, Thailand  
Contact Address: 8/81, Phahonyothin 54, Ngamwongwan road, Ladyao,  
Chatuchak, Bangkok 10900, Thailand

## Education:

2013 B.Sc. Chemistry, Kasetsart University, Thailand  
2016 M. Sc. Chemistry, Chulalongkorn University, Thailand

## Conferences:

January 21-23, 2015 Pure and Applied Chemistry International  
Conference 2015, Thailand.  
December 15-20, 2015 The 2015 International Chemical Congress of  
Pacific Basin Societies, USA.  
February 9-1, 2016 Pure and Applied Chemistry International  
Conference 2016, Thailand.

## Proceeding:

Sukmanee, T.; Wongravee, K.; Ekgasit, S.; Thammacharoen, C.;  
Pienpinijtham, P., Azo coupling-based surface enhanced Raman  
scattering for a facile detection of carbofuran, Proceedings of  
Pure and Applied Chemistry International Conference 2016  
(PACCON2016), Bangkok, Thailand.

## Scholarship and Awards:

2007-present The development and Promotion of Science and